



UNIVERSITÀ
POLITECNICA
DELLE MARCHE

FACOLTÀ DI INGEGNERIA

CORSO DI LAUREA MAGISTRALE IN INGEGNERIA MECCANICA

**Sviluppo di una procedura per l'ottimizzazione del
modello numerico di una pala eolica mediante il
confronto con i dati sperimentali**

**Development of an optimization procedure for the
updating of the model of a wind turbine blade**

Candidate:

Paola Di Mascio

Advisor:

Prof. Paolo Castellini

Coadvisor:

Dr. Eng. Emilio Di Lorenzo

Academic Year 2019-2020



UNIVERSITÀ
POLITECNICA
DELLE MARCHE

FACOLTÀ DI INGEGNERIA

CORSO DI LAUREA MAGISTRALE IN INGEGNERIA MECCANICA

**Sviluppo di una procedura per l'ottimizzazione del
modello numerico di una pala eolica mediante il
confronto con i dati sperimentali**

**Development of an optimization procedure for the
updating of the model of a wind turbine blade**

Candidate:

Paola Di Mascio

Advisor:

Prof. Paolo Castellini

Coadvisor:

Dr. Eng. Emilio Di Lorenzo

Academic Year 2019-2020

UNIVERSITÀ POLITECNICA DELLE MARCHE
FACOLTÀ DI INGEGNERIA
CORSO DI LAUREA MAGISTRALE IN INGEGNERIA MECCANICA
Via Brezze Bianche – 60131 Ancona (AN), Italy

Acknowledgments

I would like to acknowledge the entire DTU team for providing the experimental data obtained in the tests carried out on the blade, and the finite element model of the blade. I would also offer my gratitude to Siemens PLM Software for this very interesting internship experience and to my supervisor Emilio Di Lorenzo for his great support and willingness.

Ancona, Ottobre 2020

Paola Di Mascio

The work presented in this thesis was performed at
Siemens Industry Software NV, Test Division
Leuven, Belgium.

Sommario

La procedura di certificazione delle pale delle turbine eoliche, regolata dallo standard internazionale IEC 61400-23, prevede che tutti i prototipi siano soggetti a test strutturali in piena scala, che comprendono: test di carico, per verificare la resistenza strutturale della pala, test a fatica, per verificare che la pala sia in grado di raggiungere una vita utile di almeno 25 anni, e test dinamici per la determinazione di alcune delle frequenze naturali. Tuttavia, a causa della tendenza a costruire pale sempre più lunghe, i requisiti previsti dalla norma non sembrano essere più sufficienti per assicurare l'affidabilità di queste strutture che sono sempre più flessibili e che arrivano a rottura molto più facilmente. L'oggetto della presente tesi è pertanto quello di cercare di ottenere una conoscenza più approfondita della dinamica strutturale di una pala eolica, rispetto a quanto richiesto dalla norma. In particolare possono essere individuate 4 fasi principali dello studio:

1. analisi modale sperimentale;
2. analisi modale numerica;
3. correlazione tra risultati sperimentali e numerici;
4. aggiornamento del modello numerico.

L'analisi modale sperimentale è stata eseguita a partire dai dati sperimentali forniti dal Dipartimento dell'Energia Eolica della DTU, *Danmarks Tekniske Universitet*, relativi a test di analisi modale effettuati su una pala eolica in due diverse condizioni:

- durante il test a fatica, il che significa che la pala veniva stoppata durante il test a fatica per poter effettuare test modali a diversi livelli di fatica;
- prima del test a fatica, quindi sulla pala non danneggiata.

I parametri modali ottenuti dall'analisi dei dati derivati dai test effettuati a diversi livelli di fatica sono stati confrontati tra loro per vedere se ci fossero variazioni dovute al danno a fatica subito dalla pala. In generale si può dire che da questo confronto

non sono emerse variazioni significative dei parametri modali che possano permettere l'identificazione di un danno, e l'unica variazione degna di nota è rappresentata dalla suddivisione di un modo in due nel passaggio dal terzo al quarto livello di fatica nel caso di test con martello modale (vedi figura 4.11).

Mentre i parametri modali ottenuti dall'analisi dei dati sperimentali derivanti dai test effettuati sulla pala intatta, sono stati utilizzati come riferimento per la validazione del modello numerico della pala e per il suo successivo aggiornamento. Il modello numerico della pala era stato originariamente creato usando il software commerciale MSC Patran[®] e il software interno della DTU chiamato Blade Modelling Tool (BMT); dopodichè è stato importato in Simcenter 3D[®] ed è stato risolto utilizzando "SOL 103 Real Eigenvalues" in modo da ottenere i parametri modali. In questo modo è stato possibile calcolare la correlazione tra risultati numerici e sperimentali. Infine il modello numerico è stato aggiornato allo scopo di migliorare la correlazione con i dati sperimentali tramite il software HEEDS[®], che permette di risolvere problemi di ottimizzazione. In particolare sono state effettuate due diverse ottimizzazioni: la prima con il solo obiettivo di ridurre la differenza tra le frequenze naturali stimate a partire dai dati sperimentali e quelle ottenute dal modello numerico, mentre la seconda con gli ulteriori obiettivi di massimizzazione dei valori del MAC; e in entrambi i casi come variabili di progetto sono state scelte la densità e i moduli di Young di 3 dei 7 materiali costituenti la pala. Nella prima ottimizzazione la soluzione trovata dall'algoritmo per ridurre la differenza tra le frequenze naturali è stata quella di minimizzare le densità e massimizzare i moduli di Young di tutti i materiali (vedi tabella 4.2a e figura 5.12). Ciò è dovuto al fatto che inizialmente le frequenze naturali del modello numerico erano inferiori rispetto a quelle ricavate sperimentalmente, per cui l'algoritmo ha cercato di ridurre tale differenza incrementando le frequenze naturali derivanti dal modello numerico tramite un aumento della rigidezza del modello stesso. Tuttavia in questo modo si ottiene che il MAC peggiora in quasi tutti i casi, ed è per questo che si è scelto di realizzare anche una seconda ottimizzazione aggiungendo l'obiettivo della massimizzazione del MAC. Quindi, con la seconda ottimizzazione è stato possibile ottenere sia una riduzione della differenza tra le frequenze naturali, sia un miglioramento del valore del MAC. Tuttavia il miglioramento ottenuto non è molto significativo, a causa del

basso numero di iterazioni effettuate con l'algoritmo, per cui un possibile sviluppo futuro potrebbe essere quello di provare a ripetere l'ottimizzazione con un maggior numero di iterazioni, così come anche aggiungendo variabili di progetto.

Abstract

This thesis concerns the experimental structural dynamics identification and structural model validation of a 14.3m long research blade.

In particular, four successive phases of the study may be identified:

- experimental modal analysis,
- numerical modal analysis,
- correlation between experimental and simulation results,
- model updating.

The experimental modal analysis was carried out on the basis of the experimental data provided by the Wind Energy Department of DTU (*Danmarks Tekniske Universitet*) related to modal tests carried out on the blade under two different conditions:

- during the fatigue test, which means that the blade was stopped during the fatigue test in order to perform modal tests at different levels of fatigue cycles;
- before the fatigue test, so on the undamaged blade.

The modal parameters obtained from the analysis of the data derived from the tests carried out at different levels of fatigue cycles were compared to each other to see if there was any variation due to the fatigue damage suffered by the blade. While the results coming from the analysis of the data related to the tests performed on the undamaged blade were used as a reference to validate the FE model of the blade and then to update it in order to improve the correspondence between test and simulation results.

Contents

Introduction	xv
I. Theoretical background	1
1. Modal Analysis	3
1.1. Theoretical modal analysis	4
1.1.1. Single-Degree-of-Freedom (SDOF) systems	5
1.1.2. Multiple-Degree-of-Freedom (MDOF) systems	12
2. Experimental modal analysis	16
2.1. EMA vs OMA approach	16
2.2. Modal parameters estimation	18
2.3. Modal model validation	21
2.4. Model validation	22
3. Digital Signal Processing	23
3.1. Data acquisition	23
3.1.1. Sampling	23
3.1.2. Quantization	28
II. Blade case	29
4. Modal analysis during fatigue test	32
4.1. Pull and Release tests	32
4.1.1. Experimental setup	33
4.1.2. Data analysis	33
4.1.3. Results	36

4.2. Hammer tests	39
4.2.1. Experimental setup	39
4.2.2. Data analysis and Results	39
5. Structural dynamic analysis on the undamaged blade	47
5.1. Experimental modal analysis	47
5.1.1. Experimental setup	47
5.1.2. Data analysis and Results	49
5.2. Finite element analysis	52
5.3. Correlation between experimental and simulation results	54
5.4. Model updating	57
5.4.1. First optimization	57
5.4.2. Second optimization	61
6. Conclusions and future works	64

List of Figures

1.1. Example of a SDOF system	5
1.2. Plot of the Real (up) and Imaginary (down) part of the Receptance	9
1.3. Plot of the Amplitude and Phase of the Receptance	10
1.4. Double logarithmic graph of the receptance as a function of frequency	10
1.5. 3dB method	12
2.1. Assumptions underlying OMA, figure retrieved from [1]	17
3.1. Effect of aliasng on the spectrum of the reconstructed signal	25
3.2. Reconstructed signal when acquisition time is equal (a) or not (b) to the period of oscillation of the signal	26
3.3. Effect of Leakage on the spectrum of the reconstructed signal	27
4.1. Photo of the experimental setup of the pull and release tests	33
4.2. Example of a Crosspower Sum obtained in one of the Pull & Release Test	35
4.3. MAC matrices between the Pull and Release tests	38
4.4. Example of a FRFs Sum obtained in one of the Hammer Tests	39
4.5. Stabilization Diagram from the hammer test performed at 4.5×10^5 fatigue cycles	40
4.6. Stabilization Diagram from the hammer test performed at 1.1×10^6 fatigue cycles	40
4.7. Stabilization Diagram from the hammer test performed at 1.5×10^6 fatigue cycles	41
4.8. FRFs at 4.5×10^5 fatigue cycles	41
4.9. FRFs at 1.1×10^6 fatigue cycles	41
4.10. FRFs at 1.5×10^6 fatigue cycles	42

4.11. Overlay of the FRF Sum functions coming from the 4 hammer tests	44
4.12. MAC matrices between the Hammer tests	45
5.1. Instrumented blade on the test stand in the free-free support configuration	48
5.2. Excitation points and sensors	48
5.3. Sensors placed in each station	48
5.4. Stabilization chart obtained with Polymax algorithm in the chosen frequency-band	49
5.5. FRFs from Station 1	50
5.6. Finite element model of the blade in Simcenter3D®	52
5.7. Values of the properties of the materials used in the model	53
5.8. MAC matrix from the 1 st correlation	54
5.9. COMAC graphs before and after removing problematic sensors . . .	55
5.10. MAC graphs before (a) and after (b) removing problematic sensors .	55
5.11. Frequency difference before (a) and after (b) 1 st optimization	58
5.12. Graph of the design variables values in all designs of the 1 st optimization	60
5.13. Frequency difference before (a) and after (b) 2 nd optimization	61
5.14. Graph of the design variables values in all designs of the 2 nd optimization	63

List of Tables

4.1. Mode sets from Pull and Release test at 4.5×10^5 (a), 1.1×10^6 (b), 1.5×10^6 (c) and 2×10^6 (d) cycles	36
4.2. Frequency and Damping difference between P&R tests	37
4.3. Mode sets obtained from the hammer tests at 4.5×10^5 (a), 1.1×10^6 (b), 1.5×10^6 (c) and 2×10^6 (d) cycles	43
4.4. Frequency and Damping difference between Hammer tests	46
5.1. Final mode set from the EMA on the undamaged blade	51
5.2. MAC values before and after removing problematic sensors	56
5.3. Frequency difference before and after 1 st optimization	59
5.4. MAC variation after 1 st optimization	59
5.5. Values of the design variables before and after 1 st optimization	60
5.6. Frequency difference before and after 2 nd optimization	62
5.7. MAC variation after 2 nd optimization	62
5.8. Values of the design variables before and after 1 st optimization	63

Introduction

As part of the certification procedure, contained in the IEC 61400-23 standard [2], all wind turbine blade prototypes must be subjected to a full-scale structural testing which includes load carrying capacity under extreme loading to verify the structural strength of the blade, test of fatigue resistance to ensure that the blade will be reaching the designed lifetime of about 25 years, and dynamic tests aimed at the determination of some of the natural frequencies. [3] To be precise, the standard requires the identification of only the first and second flapwise and of the first edgewise natural frequencies, while the identification of the other modal properties, i.e. damping and the mode shapes, is listed under the optional tests. However, considering the nowadays tendency to increase the length of the wind turbine blades, which can exceed 100 meters in the offshore applications, the requirements of the standard turn out to be not enough to ensure the reliability of such flexible structures, that can come more easily to failure. This determined the need for a more accurate dynamic investigation of the blades because a deeper understanding of the dynamic behavior is crucial to better analyze stability problems and failure modes.

This can be obtained by adding the determination of the mode shapes to the traditional characterization, and increasing the number of natural frequencies to identify. The modal parameters of the blades, that is natural frequencies, damping and mode shapes, can be determined by means of the modal analysis, which is the most common method to characterize the dynamic properties of a mechanical system.[4]

The first purpose of this study was to perform several modal tests on a 14,3m long research blade, in order to analyze its dynamic behavior in two different situations. In particular the first set of tests was performed on the undamaged blade, while the second set was carried out during the fatigue test of the blade, which means that the

Introduction

blade was stopped at four different number of fatigue cycles to perform the modal tests.

In the first case the blade was excited with two electrodynamic shakers, so the data coming from these tests were processed according to the principles of the Experimental Modal Analysis (EMA) in order to identify the modal parameters of the blade, exceeding the requirements of the standard.

In the second case the blade was subjected to two different kinds of test everytime it was stopped: hammer test and pull and release test. So the data coming from the pull and release test were processed according to the principles of the Operational Modal Analysis (OMA) while those coming from the hammer test were processed according to the principles of EMA.

The purpose of the first tests was to obtain a deep knowledge of the dynamic of the blade, while those performed during the fatigue test were aimed at the identification of the fatigue damage of the blade by the comparison of the modal parameters obtained at the different fatigue levels.

In addition to the experimental tests, the second purpose of this study was that of the comparison between numerical and experimental results aimed at the updating of the FE model of the blade to improve the correlation. This second analysis was performed using only the data coming from the experimental tests of the undamaged blade.

Part I.

Theoretical background

Chapter 1.

Modal Analysis

Modal analysis is a key technology in structural dynamics analysis, and, more precisely, it is the process of determining the mathematical model of the dynamics of a structure in terms of its vibration characteristics.

In particular modal analysis expresses the vibration response of a linear time-invariant dynamic system as a linear combination of its resonant modes, since they are inherent properties of the structures.

The resonant modes of a structure are the vibrations that characterize the structure at its resonances and resonance is the phenomenon of excessive amplification of the vibration response of a structure which happens when it is excited by a force at one of its natural frequencies, and can result in possible damage, discomfort and malfunctioning.

Each resonance mode is defined by a natural frequency, damping ratio and characteristic displacement pattern, namely mode shape. These data are known as the *modal parameters* of the structure, and they are determined in order to formulate the mathematical model of its dynamic behaviour, known as *modal model*. Once the modal model of the structure is known it is also possible to determine its *response model*, which describes the relationship between the force applied to the system and its subsequent response to it.

Modal analysis can be carried out using two different approaches:

- *Theoretical modal analysis*;
- or *Experimental modal analysis*.

The first one aims at obtaining the modal model of the structure by knowing its physical properties, like mass, damping and stiffness, while the other consists in determining the modal model of the structure by measuring its vibrational responses.

But the modal model is often not the final objective of the study because it can be used for further applications:

- *Response prediction*: which means predicting the response of the structure to a given dynamic loading of interest, that could be the one the structure is subjected to during its real-life operating conditions;
- *Sensitivity analysis*: predicting the effect of structural modifications to the dynamic behavior of the structure;
- *Model updating*: changing the initial values chosen for the material properties and boundary conditions in the numerical model of the structure trying to improve the correspondence with the experimental results. [5]

1.1. Theoretical modal analysis

The theoretical vibration analysis consists in three successive stages:

- setting up the governing equations of motion;
- performing a free vibration analysis using the equations of motion;
- forced response analysis, and in particular that for harmonic excitation. In fact these particular kind of responses are the quantities which we are most likely to be able to measure in practice.

Although very few practical structures could realistically be modelled by a single-degree-of-freedom (SDOF) system, the properties of such a system are very important because those for a more complex multidegree-of-freedom (MDOF) system can always be represented as the linear superposition of a number of SDOF characteristics. So it is better to start analyzing the theoretical modal analysis considering the case of the SDOF systems. [6]

1.1.1. Single-Degree-of-Freedom (SDOF) systems

A simple example of a single-degree-of-freedom system could be a mass m connected to the wall by a spring and a damper, and which can run parallel to the ground.

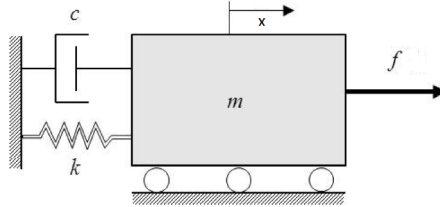


Figure 1.1.: Example of a SDOF system

The dynamic of such a system vibrating under the action of an external force f can be expressed applying the second Newton law:

$$m\ddot{x}(t) + c\dot{x}(t) + kx(t) = f(t) \quad (1.1)$$

Where c is the damping ratio, k is the stiffness, x is the displacement of the system, so $m\ddot{x}$ is the inertial force, $c\dot{x}$ is the damping force and kx is the elastic force of the spring.

As first step of the theoretical modal analysis of this system we need to search for its free vibration response. The equation of motion for free vibrations becomes:

$$m\ddot{x}(t) + c\dot{x}(t) + kx(t) = 0 \quad (1.2)$$

If we use the trial solution $x(t) = Xe^{i\omega t} = Xe^{st}$ we obtain:

$$(ms^2 + cs + k) = 0 \quad (1.3)$$

This, in turn, leads to:

$$s_{1,2} = -\frac{c}{2m} \pm \frac{\sqrt{c^2 - 4km}}{2m} = -\omega_n\zeta \pm i\omega_n\sqrt{1 - \zeta^2} \quad (1.4)$$

Where:

$$\omega_n = \sqrt{\frac{k}{m}} \quad (1.5)$$

$$\zeta = \frac{c}{2\sqrt{km}} \quad (1.6)$$

are respectively named *natural frequency* and *damping ratio*. So this means that the free vibration response of the system can be expressed as:

$$x(t) = A_1 e^{s_1 t} + A_2 e^{s_2 t} \quad (1.7)$$

Where the values of A_1 and A_2 are constants which depend upon the initial conditions. It is important to underline that depending on the value of $\zeta^2 - 1$ three different responses of the system can be obtained:

- if $\zeta = 1$ then $s_{1,2} = -\omega_n$, so the response of the system becomes:

$$x(t) = (A_1 + A_2)e^{-\omega_n t} = Ae^{-\omega_n t} \quad (1.8)$$

which means that there is no oscillatory motion in this case, but an exponential decay of motion over time.

- if $\zeta > 1$ then $s_{1,2} = -\omega_n \zeta \pm \omega_n \sqrt{\zeta^2 - 1}$, so the response of the system becomes:

$$x(t) = A_1 e^{(-\zeta + \sqrt{\zeta^2 - 1})\omega_n t} + A_2 e^{(-\zeta - \sqrt{\zeta^2 - 1})\omega_n t} \quad (1.9)$$

which means that also in this case there is no oscillatory motion but an exponential decay of motion over time.

- if $\zeta < 1$ then $s_{1,2} = -\omega_n \zeta \pm i\omega_n \sqrt{1 - \zeta^2}$ so the free vibration response of the system becomes:

$$x(t) = A_1 e^{(-\zeta + i\sqrt{1 - \zeta^2})\omega_n t} + A_2 e^{(-\zeta - i\sqrt{1 - \zeta^2})\omega_n t} \quad (1.10)$$

Which can be also written as:

$$x(t) = Ae^{-\zeta\omega_n t} \sin\left(\sqrt{1 - \zeta^2}\omega_n t + \phi\right) \quad (1.11)$$

So this motion can be considered as composed of:

- an imaginary oscillatory part, with a frequency of $\omega_d = \omega_n \sqrt{1 - \zeta^2}$;

– a real part of exponential decay.

Since we are studying the vibrational behaviour of the system we'll be considering only the latter kind of motion, so the one that happens if $\zeta < 1$.

Lastly, to complete the theoretical modal analysis of the SDOF system, we perform the forced vibration analysis.

If the external force applied to the mass is harmonic: $f(t) = Fe^{i\omega t}$ then the solution of the equation will be like $x(t) = Xe^{i\omega t}$. So the equation of motion (1.1) becomes:

$$(-m\omega^2 + ic\omega + k)X = F \quad (1.12)$$

From this last equation we can easily obtain the response function of the system (which is the one that expresses the relationship between the force applied to the system and its response) by highlighting the ratio between displacement and force:

$$\frac{X}{F} = \alpha(\omega) = \frac{1}{-m\omega^2 + ic\omega + k} \quad (1.13)$$

Since the (1.13) is written in the frequency domain it takes the name of *Frequency Response Function (FRF)* of the system and, in particular, this kind of FRF is defined as *Receptance* because it is defined in terms of displacement. At this point it is worth to examine in depth this response function in order to understand the influence of the physical characteristics and modal parameters of the system upon its vibrational response. For this purpose we start rewriting the (1.12) in terms of the natural frequency ω_n and the damping ratio ζ :

$$\left(-\frac{\omega^2}{\omega_n^2} + i\frac{\omega}{\omega_n}2\zeta + 1\right) = \frac{F}{k} \quad (1.14)$$

So the FRF becomes:

$$\alpha(\omega) = FRF = \frac{X}{F} = \frac{\frac{1}{k}}{\left[1 - \left(\frac{\omega}{\omega_n}\right)^2\right] + 2i\zeta\frac{\omega}{\omega_n}} = \frac{\frac{1}{k} \left\{ \left[1 - \left(\frac{\omega}{\omega_n}\right)^2\right] - 2i\zeta\frac{\omega}{\omega_n} \right\}}{\left[1 - \left(\frac{\omega}{\omega_n}\right)^2\right]^2 + 4\zeta^2\left(\frac{\omega}{\omega_n}\right)^2} \quad (1.15)$$

We can see that the FRF is a complex function so its real and imaginary part can be studied separately.

Chapter 1. Modal Analysis

The real part of the Receptance is:

$$Re[\alpha(\omega)] = \frac{\frac{1}{k} \left[1 - \left(\frac{\omega}{\omega_n} \right)^2 \right]}{\left[1 - \left(\frac{\omega}{\omega_n} \right)^2 \right]^2 + 4\zeta^2 \left(\frac{\omega}{\omega_n} \right)^2} \quad (1.16)$$

While the imaginary part is:

$$Im[\alpha(\omega)] = \frac{-\frac{2\zeta}{k} \frac{\omega}{\omega_n}}{\left[1 - \left(\frac{\omega}{\omega_n} \right)^2 \right]^2 + 4\zeta^2 \left(\frac{\omega}{\omega_n} \right)^2} \quad (1.17)$$

Analyzing the function that describes the real part of the Receptance we can deduce that:

- (a) if $\omega = 0$ then $Re[\alpha] = \frac{1}{k}$
- (b) if $\omega = \omega_n$ then $Re[\alpha] = 0$
- (c) if $\omega \rightarrow \infty$ then $Re[\alpha] \rightarrow 0$

Whereas, analyzing the function that describes the imaginary part we can deduce that:

- (a) if $\omega = 0$ then $Im[\alpha] = 0$
- (b) if $\omega = \omega_n$ then $Im[\alpha] = -\frac{1}{2k\zeta}$
- (c) if $\omega \rightarrow \infty$ then $Im[\alpha] \rightarrow 0$

This means that at resonance the trend of the function is governed by the damping, and if the damping is zero the imaginary part of the function goes to ∞ , which is the condition of ideal resonance. So through the visual analysis of the imaginary part of the receptance function we can recognize the resonance peak:

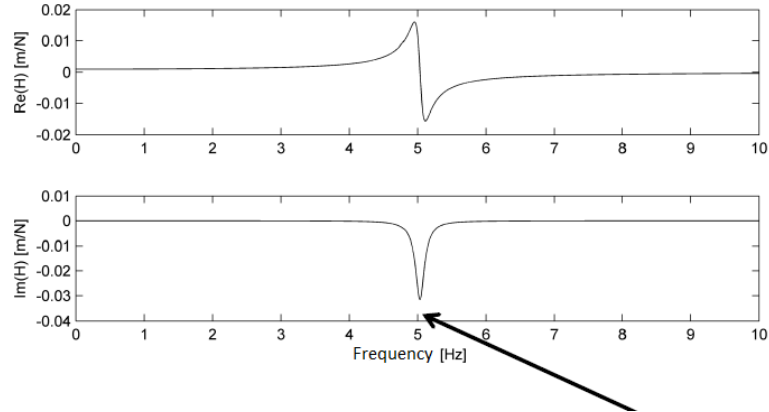


Figure 1.2.: Plot of the Real (up) and Imaginary (down) part of the Receptance

The same informations can be extracted if we consider the amplitude and the phase of the Receptance. The amplitude is defined as:

$$|\alpha(\omega)| = \sqrt{\text{Re}^2[\alpha(\omega)] + \text{Im}^2[\alpha(\omega)]} = \frac{\frac{1}{k}}{\sqrt{\left[1 - \left(\frac{\omega}{\omega_n}\right)^2\right]^2 + 4\zeta^2 \left(\frac{\omega}{\omega_n}\right)^2}} \quad (1.18)$$

And the phase is:

$$\angle\alpha(\omega) = \arctan \frac{\text{Im}[\alpha(\omega)]}{\text{Re}[\alpha(\omega)]} = \arctan \frac{-2\zeta \frac{\omega}{\omega_n}}{1 - \left(\frac{\omega}{\omega_n}\right)^2} \quad (1.19)$$

Studying the function that describes the amplitude of the Receptance we can deduce that:

- (a) if $\omega = 0$ then $|\alpha| = \frac{1}{k}$
- (b) if $\omega = \omega_n$ then $|\alpha| = \frac{1}{2k\zeta}$
- (c) if $\omega \rightarrow \infty$ then $|\alpha| \rightarrow 0$

And studying the function that describes the phase of the Receptance we can deduce that:

- (a) if $\omega = 0$ then $\angle\alpha = 0$
- (b) if $\omega = \omega_n$ then $\angle\alpha = -90^\circ$

(c) if $\omega \rightarrow \infty$ then $\angle\alpha = -180^\circ$

This means that through the visual analysis of the amplitude of the receptance function we can recognize the resonance peak:

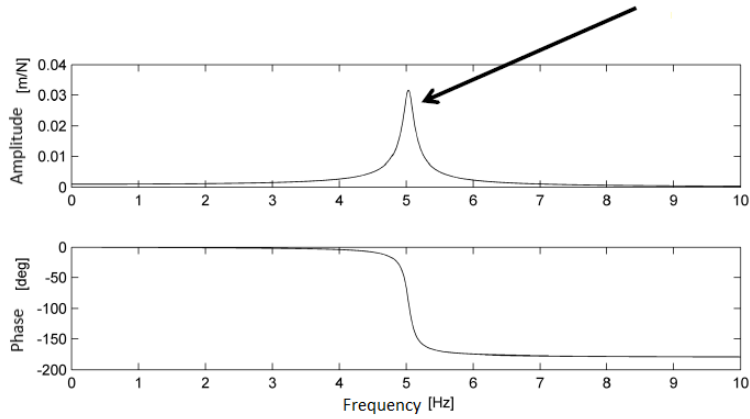


Figure 1.3.: Plot of the Amplitude and Phase of the Receptance

Moreover, if we consider the (1.1), we can observe that:

- if $\omega = 0$ then $\ddot{x} = -\omega^2 X = 0$, $\dot{x} = i\omega X = 0$ and therefore $kx = F$. So, since the phase is zero for $\omega = 0$, this means that the external force is completely balanced by the spring elastic force;
- if $\omega = \omega_n$ and we consider the (1.14) then we get that $i2\zeta = \frac{F}{k}$. So, since the FRF's phase is -90° and there is an i , the external force is completely balanced by the damping force;
- if $\omega \rightarrow \infty$ and considering that $\ddot{x} = -\omega^2 X$ and $\dot{x} = i$, we can neglect the term containing \dot{x} because it is an infinity of lower order, and say that $m\ddot{x} = -m\omega^2 X = F$. So, since the phase of the FRF is -180° , the external force is completely balanced by the inertial force.

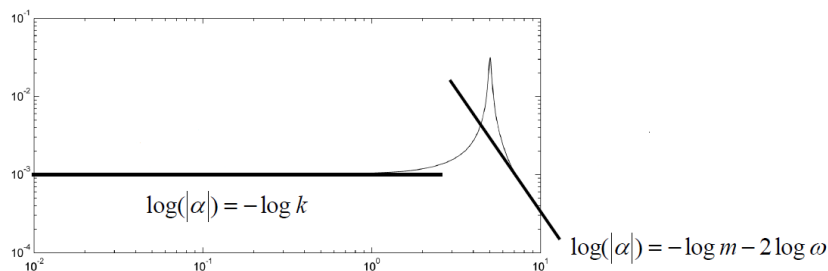


Figure 1.4.: Double logarithmic graph of the receptance as a function of frequency

1.1. Theoretical modal analysis

These considerations can also be highlighted graphically if we consider the double logarithmic graph of the amplitude of the Receptance as a function of frequency. In fact we can see that:

- if $\omega = 0$ then $\log(|\alpha|) = -\log k$, so the FRF at the low frequencies in the double logarithmic graph can be approximated by a straight line parallel to the frequency axis, which is called *stiffness line*;
- if $\omega \rightarrow \infty$ then $\log(|\alpha|) = -\log m - \log \omega^2 = -\log m - 2 \log \omega$, so the FRF at the high frequencies in the double logarithmic graph can be approximated by a straight line with a negative slope, which is called *mass line*.

So we can see that from the FRF's graph it is possible to obtain the stiffness and the mass of the system, at low and high frequencies respectively. In the resonance region, where the FRF is dominated by the damping, it is possible to use the graph of the FRF's amplitude in order to obtain the value of the damping ratio. The method that is used for this purpose is called *half-power method*, and the procedure proposed by this method consists of the following steps:

1. determination of the resonance frequency ω_n , which is the one corresponding to the peak in the FRF;
2. determination of the frequency band in which the maximum value of the FRF, i.e. the value of the FRF for $\omega = \omega_n$, is halved;
3. now it is possible to calculate the damping ratio ζ as $\zeta = \frac{\omega_2 - \omega_1}{2\omega_n}$, where ω_1 and ω_2 are the extreme frequencies of the band determined in the previous step.

This method is also known as *3dB method* because the frequencies ω_1 and ω_2 corresponds to the points where there is a decrease in amplitude of the FRF equal to 3dB. In fact, if we calculate the ratio between the value of the FRF at ω_n and at ω_1 or ω_2 , where its power halves, we obtain:

$$\frac{|H^*|}{\frac{|H^*|}{\sqrt{2}}} = \sqrt{2} \quad (1.20)$$

And, if we write the (1.20) in terms of Decibel we obtain:

$$20 \log \frac{|H^*|^2}{\frac{|H^*|^2}{\sqrt{2}}} = 20 \log \sqrt{2} = 10 \log 2 = 3dB \quad (1.21)$$

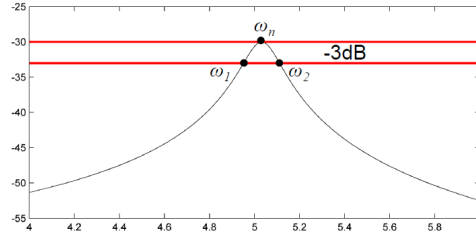


Figure 1.5.: 3dB method

1.1.2. Multiple-Degree-of-Freedom (MDOF) systems

The general equation of motion for a MDOF system with N degrees of freedom and viscous damping is:

$$[M]\{\ddot{x}(t)\} + [C]\{\dot{x}(t)\} + [K]\{x(t)\} = \{f(t)\} \quad (1.22)$$

Where:

- $[M]$ and $[K]$ are $N \times N$ mass and stiffness matrices respectively;
- $\{x(t)\}$ is a $N \times 1$ vector of time-varying displacements;
- and $\{f(t)\}$ is a $N \times 1$ vector of time-varying forces.

We will consider first the free vibration solution in order to find the natural modal properties of the system by considering the case in which $\{f(t)\} = 0$. We can assume that the equation of motion in this case admits a solution in the form:

$$\{x(t)\} = \{X\}e^{st} \quad (1.23)$$

The substitution of this solution in the (1.22) leads to:

$$(s^2[M] + s[C] + [K])\{X\} = \{0\} \quad (1.24)$$

And the non-trivial solutions of this equation are those which satisfy this condition:

$$\det[s^2[M] + s[C] + [K]] = 0 \quad (1.25)$$

The solution of this complex eigenvalue problem leads to $2N$ eigenvalues s_i that occur in complex pairs. To each of these eigenvalues corresponds an eigenvector, and also the eigenvectors occur as complex conjugates.

Therefore the solution of the problem can be described as:

$$\begin{cases} s_i, s_i^* & \text{for } i = 1 : n \\ \{\psi_i\}, \{\psi_i^*\} & \text{for } i = 1 : n \end{cases}$$

And each eigenvalue takes the same form as that obtained in the analysis of the SDOF system, that is:

$$s_i = -\omega_i \zeta_i + i\omega_i \sqrt{1 - \zeta_i^2} \quad (1.26)$$

Where ω_i and ζ_i are the natural frequency and damping ratio for the i^{th} mode. So we have converted the so-called *Spatial Model* of the system, represented by the matrices $[M]$ and $[K]$, in its *Modal Model*, constituted by two eigenmatrices, that of the eigenvalues, related to the natural frequencies, and that of the eigenvectors, that represents the mode shapes.

It is important to underline that the eigenvalues matrix is unique, while the eigenvectors matrix is not. This means that whereas the natural frequencies are fixed quantities, the mode shapes are subject to an indeterminate scaling factor which does not affect the shape of the vibration mode, only its amplitude. [6]

This is the reason why the mode shapes are always normalised in modal testing, and one of the most used normalising processes is the mass-normalisation.

In order to complete the theoretical modal analysis of the MDOF system we shall now determine the forced response solution of the system, when it is excited by a set of sinusoidal forces, all with the same frequency, ω , but with different amplitudes and phases:

$$\{f(t)\} = \{F\}e^{i\omega t} \quad (1.27)$$

As was done in the case of the free response, we can assume that the solution has

the following form:

$$\{x(t)\} = \{X\}e^{i\omega t} \quad (1.28)$$

So the equation of motion (1.22) becomes:

$$([K] - \omega^2[M] + i\omega[C])\{X\}e^{i\omega t} = \{F\}e^{i\omega t} \quad (1.29)$$

Which can be written as:

$$\{X\} = ([K] - \omega^2[M] + i\omega[C])^{-1}\{F\} \quad (1.30)$$

Where:

$$[\alpha(\omega)] = ([K] - \omega^2[M] + i\omega[C])^{-1} \quad (1.31)$$

is the $N \times N$ receptance FRF matrix for the system, and its general element $\alpha_{jk}(\omega)$ is defined as:

$$\alpha_{jk}(\omega) = \left(\frac{X_j}{F_k} \right) \quad (1.32)$$

Since the solution of $[K] - \omega^2[M] + i\omega[C] = 0$ for a single degree of freedom, as shown above, is a complex pair of eigenvalues, defined as:

$$s_{1,2} = -\omega_i\zeta_i + i\omega_i\sqrt{1 - \zeta_i^2} \quad (1.33)$$

the individual FRF can be expressed as:

$$\alpha_{jk}(\omega) = \frac{A}{i\omega - s_1} + \frac{A^*}{i\omega - s_2} \quad (1.34)$$

Where A is a constant determined by initial conditions and A^* is its complex conjugate. This means that the FRF matrix of the MDOF system could be written as:

$$\alpha(\omega) = \sum_{i=1}^N \left[\frac{A_i}{i\omega - s_1} + \frac{A_i^*}{i\omega - s_2} \right] \quad (1.35)$$

This expression constitutes the basis of modal analysis because it shows a direct correlation between the modal properties of a system and its response. In theoretical modal analysis it can be used to predict the response of a system, after performing

1.1. Theoretical modal analysis

a free vibration analysis in order to determine the modal parameters, while in experimental modal analysis it is used to determine the modal parameters of the structure from the measured FRFs.[6]

Chapter 2.

Experimental modal analysis

The experimental modal analysis (EMA), as said in the previous paragraphs, identifies a modal model from the measured forces applied to the test structure and the measured vibration responses. [5]

It is also possible to identify the modal model of a structure by knowing only its vibrational response. This is done by means of what is called *Operational Modal Analysis (OMA)*, which has the advantage to allow the analysis of the structure under its operational conditions, so the modal model identified is more realistic.

While EMA uses the FRFs to estimate the modal parameters the OMA uses the crosspowers of the vibration responses, all referred to one of the measured responses of the structure, but the curve fit process used to extract the model parameters is equivalent, so the following paragraphs will refer for convenience only to the case of the EMA.

In both cases the modal analysis consists of the following steps:

- modal parameters estimation;
- mode shapes calculation;
- modal model validation.

2.1. EMA vs OMA approach

Both EMA and OMA uses measurement data to build a mathematical model of the structure, which is then used to extract the modal parameters by an equivalent curve fit process. The main difference between the two methods lies in the way in which

the mathematical model of the structure, or system transfer matrix, is obtained. In EMA the math model of the structure is derived using the FRFs calculated from the measurements, so using a family of frequency-domain functions which express the frequency domain relationship between the inputs and the outputs for various locations around the structure. The family of FRFs contains the resonance and damping information for all the system modes, so it is used for curve-fitting, in order to obtain the synthesized FRFs. These synthesized FRFs can then be used to generate the mode shapes.

In OMA, instead, the input forces are unknown since the only available information is the system's response. So the input forces are assumed to be of the form of white noise (equal magnitude across the frequency range of interest), and spatially randomly distributed around the structure, then the responses of the structure would contain all the necessary information needed to characterize the system.

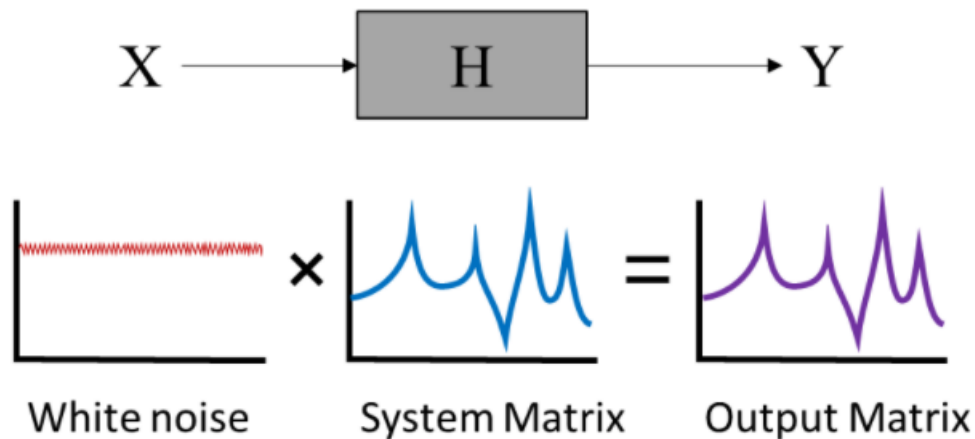


Figure 2.1.: Assumptions underlying OMA, figure retrieved from [1]

Indeed this makes the output matrix equal to the system matrix. In this case in order to highlight the dominant frequencies common between different measurement locations, autopower and crosspower spectra are used, as an alternative to the FRFs. Indeed these functions can be curve fit in the same way as the FRFs. These functions are obtained by taking the Discrete Fourier Transform of the autocorrelation and crosscorrelation function defined in the time domain. An autocorrelation function

(ACF) is the result of comparing a signal with a delayed version of itself at increasing time lags. An ACF provides a measure of the amount of correlation between the two signals. If the original signal contains periodic information (such as natural frequencies), then the delayed version of the signal will have a high amount of correlation with the original signal at certain periodicities (time lags). Similarly, a cross-correlation function compares a delayed signal to a reference signal, highlighting the periodicities common between signals from two different measurement locations. So, in order to calculate these functions, in OMA two or more reference locations are selected as reference locations.[1]

2.2. Modal parameters estimation

The parameters estimation in experimental modal analysis is based on a curve-fitting process, which consists in interpolating the measured FRF/s (or Impulse Response Function/s, IRFs) with a theoretical expression, just like the (1.35) presented in the paragraph 1.1.2. The purpose of the curve-fitting process is to determine the values of the coefficients in the theoretical expression of the FRF/s (or IRF/s) that better interpolate the measured one/s. Modal parameters identification methods can be classified into a series of different groups. First of all they can be classified according to the domain in which the analysis is carried out:

- time domain methods (which use impulse response function/s);
- frequency domain methods (which use frequency response function/s).

Generally the analysis in the frequency domain is used for the highly damped systems, because in this case the signals in the time domain contain few significant samples; while the analysis in the time domain is used for the low damped systems because in this case the signals in the time domain contain numerous significant samples. Then the methods can be divided in 2 different groups depending upon whether a single mode or several modes will be extracted at a time:

- SDOF methods;
- MDOF methods.

But it is important to underline that usually, for practical reasons, it is necessary to limit the frequency range of analysis, which means that we cannot identify the properties of the modes outside the range. But these modes influence the portion of the measured FRF considered. In particular, since at the lower frequencies the FRF can be approximated by the *stiffness line* while at the higher frequencies it can be approximated by a *mass line*, to consider this influence on FRF two additional terms, called stiffness and mass matrix, are added in the FRF equation:

$$\alpha_{jk}(\omega) = \frac{1}{\omega^2 M_{jk}^R} + \sum_{r=1}^N \frac{r A_{jk}}{\omega_r^2 - \omega^2 + i \eta_r \omega_r^2} + \frac{1}{K_{jk}^R} \quad (2.1)$$

So this is the equation used for the curve fit of the FRF, once the measured one is known. Interpolation allows the coefficients $r A_{jk}$, ω_r , η_r , M_{jk}^R and K_{jk}^R to be calculated. Once the coefficients are known, the analytical equation of the FRF, H_i , can be calculated, and it is possible to determine the error between the measured FRF, H_m , and the analytical one:

$$e_i = H_m - H_i \quad (2.2)$$

To determine the value of the coefficients we set the minimization of the quadratic error:

$$\min |e_i^2| = \min |H_m - H_i|^2 \quad (2.3)$$

Unfortunately the problem is not linear because some coefficients are in the denominator of a rational fractal function. Therefore it cannot be solved directly but through numerical algorithms that are based on assumptions and simplifications that allow to reduce the computational burden of the problem itself. A further classification relates to the number of FRFs that have to be analysed simultaneously:

- single-FRF methods;
- multi-FRF methods.

Time domain methods

The time domain methods were the first methods to be used for the modal parameters estimation. They consist in the curve fitting of the Impulse Response Function (IRF), which is the inverse Fourier transform of the FRF. These early methods are

based on an algorithm of the mathematician Prony, and are known as *Complex Exponential Methods* because they are based on the assumption that any IRF can be expressed by a series of complex exponential components, which are a function of the modal parameters. Indeed, recalling the expression of the FRF of a underdamped system with viscous damping (1.35) and the expression of each pair of conjugate solutions (1.33), the FRF can be rewritten in the form:

$$\alpha_{jk}(\omega) = \sum_{r=1}^N \frac{{}_r A_{jk}}{\omega_r \zeta + i(\omega - \omega_r \sqrt{1 - \zeta^2})} + \frac{{}_r A_{jk}^*}{\omega_r \zeta + i(\omega - \omega_r \sqrt{1 - \zeta^2})} \quad (2.4)$$

Applying the inverse Fourier transform to the FRF above we obtain the IRF:

$$h_{jk}(t) = \sum_{r=1}^N {}_r A_{jk} e^{(i\omega - s_r)t} + {}_r A_{jk}^* e^{(i\omega - s_r)t} \quad (2.5)$$

Which can be expressed as:

$$h_{jk}(t) = \sum_{r=1}^N {}_r A_{jk} e^{(\omega_r \zeta t + i(\omega - \omega_r \sqrt{1 - \zeta^2})t)} + {}_r A_{jk}^* e^{(\omega_r \zeta t + i(\omega - \omega_r \sqrt{1 - \zeta^2})t)} \quad (2.6)$$

Therefore it can be noticed that the IRF can be expressed as a series of exponential functions, the coefficients of which are the complex modal vectors while the exponents contain natural frequency and damping. In particular, this method is applied following this procedure:

1. An initial estimate of the IRFs is made for a number of degrees of freedom assumed in first approximation;
2. The FRFs are regenerated from the IRFs and compared with the measured ones. Then it is possible to calculate the error as the square of the difference between the FRF regenerated by the IRF and the measured FRF.
3. The procedure is repeated by increasing the number of degrees of freedom and the quadratic error is still calculated.
4. The error rate is displayed as a function of frequency as the number of degrees of freedom increases. When the error «stabilizes» at a minimum value you get the number of optimal degrees of freedom that are necessary to correctly

interpolate the measured data. This diagram is called Stabilization Chart.

Since also in the time domain method the quadratic error is minimized this method is called Least Square Complex Exponential method (LSCE).

Frequency domain methods

One of the major frequency domain curve fit method is *Rational Polynomial Fit*, *RPF*, which is based on the approximation of the FRF with a rational polynomial fraction:

$$\alpha_{jk}(\omega) = \frac{b_0 + b_1(i\omega) + b_2(i\omega)^2 + \dots + b_{2N-1}(i\omega)^{2N-1}}{a_0 + a_1(i\omega) + a_2(i\omega)^2 + \dots + a_{2N-1}(i\omega)^{2N-1}} \quad (2.7)$$

This method is usually applied to systems where viscous damping can be assumed. This type of curve fitting optimization is not carried out directly on the modal coefficients but on a series of polynomial coefficients that are related to modal parameters. So the determination of these parameters requires an additional step. The advantage of this method is that it can be solved as a set of linear equations and therefore in matrix form, so it is simple to solve numerically. [6]

Another important and widely used frequency domain method is the so-called PolyMAX or Polyreference Least Squares Complex Frequency Domain method, which is a non-iterative method and can be implemented in a very similar way as the industry standard polyreference (time domain) least squares complex exponential method (pLSCE), which is the LSCE applied to Multiple Input and Multiple Output (MIMO) data. [7]

2.3. Modal model validation

The modal model validation is the last step of experimental modal analysis and consists in comparing the measured and estimated FRFs and mode shapes. In order to evaluate the quality of the synthesized FRFs the softwares used for EMA provide the degree of correlation in percentage between the curves.

2.4. Model validation

After performing EMA and obtaining the modal model of the system it is possible to validate the finite element model of the structure, once it has been analyzed by a simulation software. The validation is usually carried out by comparing the natural frequencies and the mode shapes obtained in both cases. In particular the frequencies can be compared directly, while for the comparison between the mode shapes it is necessary to calculate the so-called *Modal Assurance Criterion* (MAC), which is calculated as the normalized scalar product of the two sets of vectors:

$$MAC(n) = \frac{|\{\phi_{exp}\}_n^t \{\phi_{num}\}_n|^2}{(\{\phi_{exp}\}_n^t \{\phi_{exp}\}_n)(\{\phi_{num}\}_n^t \{\phi_{num}\}_n)} \quad (2.8)$$

Where $\{\phi_{exp}\}_n$ and $\{\phi_{num}\}_n$ are the mode shapes vectors of the n^{th} mode coming from experimental and numerical models respectively. The MAC takes value between 0 (representing no consistent correspondence) and 1 (representing a consistent correspondence). Values larger than 0.9 indicate consistent correspondence whereas small values indicate poor resemblance of the two shapes. [8]

Chapter 3.

Digital Signal Processing

In order to perform an experimental modal analysis it is necessary to be able to measure the response and excitation force of the studied system. For this purpose, transducers are used, which may or may not be positioned directly on the structure, but in any case in such a way as to minimize their interference with the dynamics of the structure. These transducers measure physical quantities and give as output analog signals, that are continuous time-varying signals, but in order to be processed on the computer they must be digitized. Hence the importance of knowing the basic theory of digitization of signals if you want to make a correct acquisition of signals, and therefore a correct procedure of experimental modal analysis.

3.1. Data acquisition

An analog signal is continuous in both time and amplitude, while digital signals are discrete in both time and amplitude, so in order to convert an analog signal into a digital one there are 3 main operation that have to be done:

- *sampling*, that is discretization of time,
- *quantization*, that is discretization of amplitudes;
- and *coding*, which consists in converting the signal into a binary code.

3.1.1. Sampling

The sampling of an analog time signal consists in acquiring the value of the signal at a fixed time interval, which is known as *sampling period*, t_s . So the sampling period,

together with the acquisition time T , defines how many samples n_s of the original analog signal will be acquired:

$$n_s = \frac{T}{t_s} \quad (3.1)$$

Actually the most important parameter characterizing the sampling process is the sampling frequency, and not the sampling period, because the sampling frequency is a characteristic of the acquisition system. It can be simply defined as:

$$f_s = \frac{1}{t_s} = \frac{n_s}{T} \quad (3.2)$$

The optimal sampling frequency to choose in order to obtain a more accurate representation of the analogue signal depends on the rate of variation of the signal itself. Anyway, according to Nyquist–Shannon sampling theorem, in order to perfectly reconstruct the original continuous-time signal from the samples, the sampling rate should be higher than the double of the maximum frequency of the signal:

$$f_s \geq 2f_{max} \quad (3.3)$$

This means that the maximum frequency of the signal that can be properly reconstructed, which is known as *Nyquist frequency*, is equal to:

$$f_N = \frac{f_s}{2} \quad (3.4)$$

If the maximum frequency of the signal exceeds this value, then the so-called *Aliasing* phenomenon occurs.

Aliasing

Aliasing is one of the possible sampling errors that leads to a wrong reconstruction of the original continuous signal. It consists in the misrepresentation of those frequencies which are higher than the Nyquist one within the spectrum of the sampled signal. In particular they will appear in the spectrum of the sampled signal with a lower value, called *alias*, which can be determined as:

$$f_{Alias} = |kf_N - f_x| \quad (3.5)$$

Where k is the integer that makes f_x as close as possible to f_N , so that f_{Alias} is lower than f_N . So if the sampling rate is chosen incorrectly, in the sampled signal spectrum there will be both actual and alias frequencies, which are only the reflection of higher frequencies.

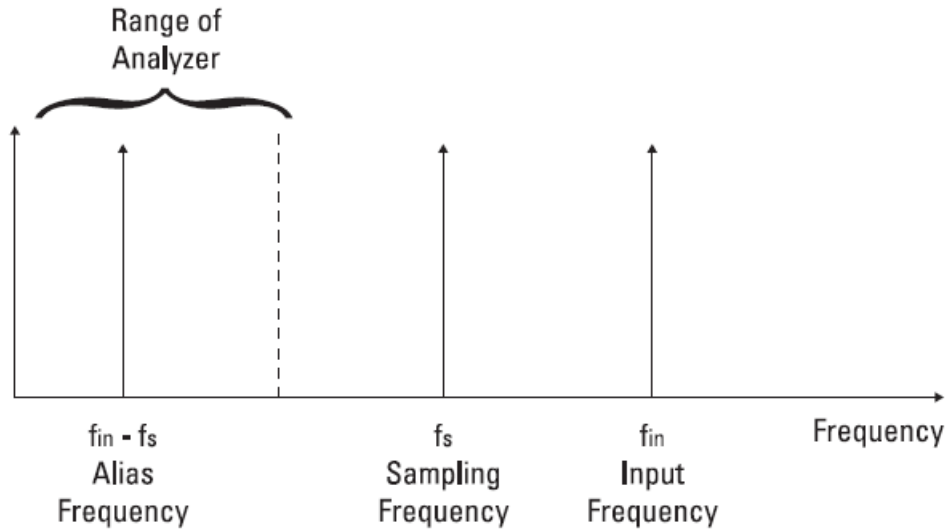


Figure 3.1.: Effect of aliasing on the spectrum of the reconstructed signal

However, once sampling has been carried out, it is no longer possible to distinguish alias frequencies from actual ones, so it is necessary to take measures to prevent aliasing before sampling. There are two ways to prevent the phenomenon of aliasing:

1. the easiest one consists in choosing a sampling frequency much bigger than the maximum frequency of the signal. However we don't always know a priori the maximum frequency of the physical phenomenon we are observing, and if you choose a very high sampling frequency you get a very small sampling period, so, if the number of the samples that can be acquired is constant, this results in a shorter acquisition time. And since the frequency resolution of the sampled signal is defined as:

$$\Delta f = \frac{1}{T} \quad (3.6)$$

this means that if T increases then the frequency resolution worsens.

2. the second and more used technique to avoid aliasing consists in the use of analog anti-aliasing filters. They are usually low-pass filters that maintain the characteristics of the original signal up to a certain cut frequency, and

eliminate all frequencies higher than that. So this method allows to eliminate the aliasing problem altogether if the cut frequency of the filter is set equal to the Nyquist frequency. Actually, due to actual filter behavior which cuts the signal gradually and not instantaneously, the cut frequency should be set to a lower value than the Nyquist frequency.

Leakage

Leakage is another phenomenon caused by an incorrect sampling that leads to a wrong reconstruction of the original signal. In particular it consists in a misrepresentation of the spectrum of the analog signal and it is related to the process of conversion of the sampled signal from the time domain to the frequency domain, which is done by means of the *Fast Fourier Transform, FFT*. FFT is based on the assumption that every signal is periodic with a period of oscillation equal to the acquisition time, therefore if the acquisition time does not coincide with the period of oscillation of the signal, discontinuities are artificially introduced in the reconstructed signal in the time domain causing a modification of the signal also in the frequency domain.

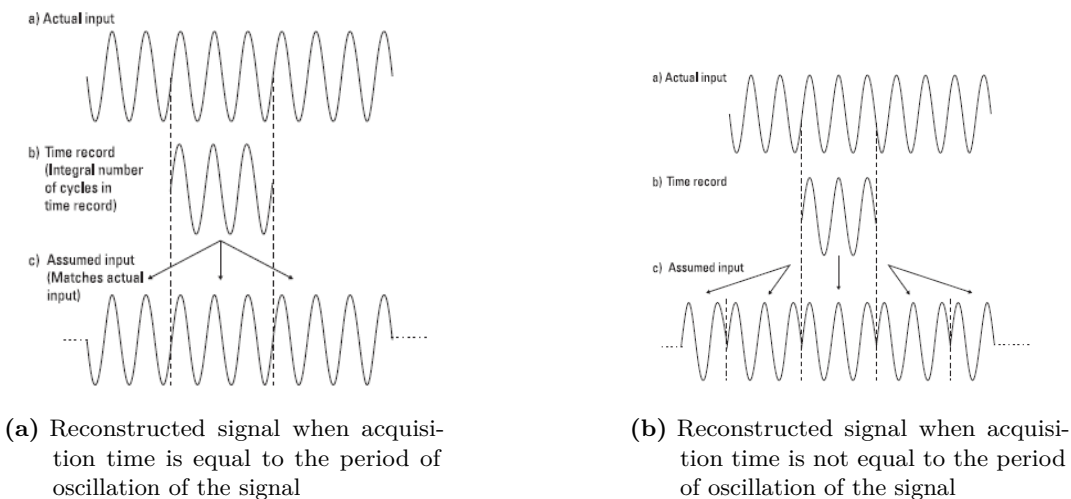


Figure 3.2.: Reconstructed signal when acquisition time is equal (a) or not (b) to the period of oscillation of the signal

More precisely because of Leakage the spectrum is no longer constituted by a peak at a single frequency, but by a lower and wider bell-shaped curve, so this phenomenon involves a misrepresentation of both the frequency, due to peak enlargement, and the amplitude, due to peak lowering. In summary it can be said that leakage affects the

spectrum of the signal reconstructed causing a different distribution of the spectral lines, and in particular:

- there will be new components, not linked to the original signal but to the discontinuities created in the reconstructed signal because of the difference between the acquisition time and the period of oscillation of the signal;
- the energy of the signal is no longer associated with a single frequency but it is distributed over multiple frequencies.

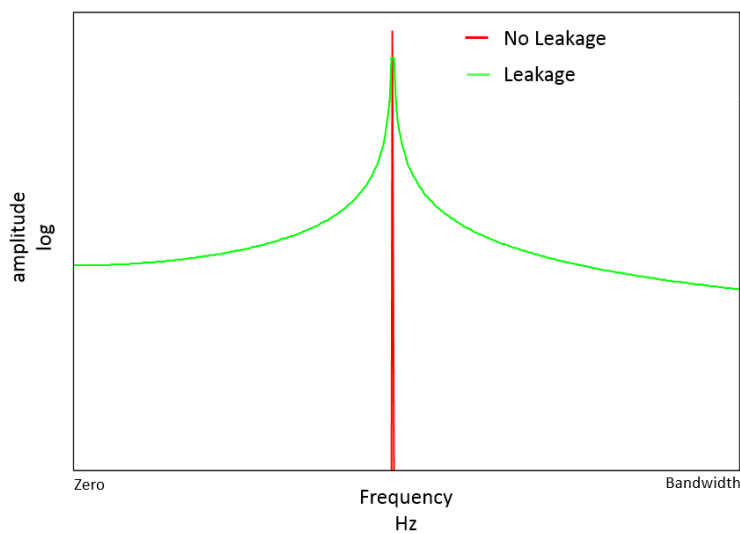


Figure 3.3.: Effect of Leakage on the spectrum of the reconstructed signal

There are 3 different ways to reduce the effect of Leakage:

1. acquire the signal for a time equal to the period of oscillation of the signal;
2. acquire the signal for a much longer time than the period of oscillation of the signal;
3. window the signal.

The first method is an impractical method because usually the period of oscillation of the signal is not known a priori. The second method does not eliminate the leakage but limits it because it averages the error introduced on a very large statistical basis. The third method is the most common one and it consists in multiplying the signal by a function called "*window*" because it goes to zero at the end of a time window. More precisely these functions should be such as to change the signal amplitude

at the end of the time window so as to reduce the effect of discontinuities. In this way you obtain a signal different from the original in terms of shape in the time domain but more similar to the original with regard to the spectrum. Anyway, since windows modify the amplitude of the signal in the time domain, then they will have to be compensated with appropriate correction coefficients which can be found in literature.

3.1.2. Quantization

The quantization of the amplitudes of the signal depends on two characteristics of the acquisition system:

- the number of bits, n_b ;
- and the full scale $V_{max} - V_{min}$.

More precisely the number of bits determines the number of representable amplitude levels n_l , since they are defined as:

$$2^{n_b} = n_l \quad (3.7)$$

while the amplitude resolution of the signal, ΔV can be determined as:

$$\Delta V = \frac{V_{max} - V_{min}}{n_l} \quad (3.8)$$

[9]

Part II.

Blade case

Introducion

This second part of the thesis is about the experimental and numerical analysis of the blade. The blade under study is a 14,3m long research blade entirely designed at DTU (*Danmarks Tekniske Universitet*) Wind Energy Department and manufactured by Olsen Wings. It was tested at the Large Scale Test Facility built for the experimental research of full-scale wind turbine blades and its subcomponents, at DTU Wind Energy department. Therefore this study is based on the experimental data provided by DTU.

As mentioned before the analysis carried out on the blade consists of three main parts:

- analysis of the experimental data coming from the modal tests performed during the fatigue test of the blade;
- analysis of the experimental data coming from the modal tests performed on the undamaged blade;
- numerical analysis of the undamaged blade which includes the correlation between experimental and simulation data and the subsequent model updating.

Chapter 4.

Modal analysis during fatigue test

This chapter is about the analysis of the experimental data coming from the modal tests performed on the blade during its fatigue test, which means that the blade was stopped several times during its fatigue resistance test so that the modal tests could be carried out. In particular the blade was stopped four times at the following numbers of fatigue cycles:

Test	Fatigue cycles
1	4.5×10^5
2	1.1×10^6
3	1.5×10^6
4	2×10^6

And each of these times two different types of tests have been done:

- Pull and Release tests;
- Hammer tests.

4.1. Pull and Release tests

The pull and release tests consisted in pulling the tip of the blade towards the floor and releasing it once it had reached the desired displacement, to measure the free vibration response. Since in this kind of tests the excitation is unknown, the measured data were analyzed according to the principles of Operational Modal Analysis.

4.1.1. Experimental setup

During these tests the blade was clamped to a rigid block through the circular interface plate in a flapwise configuration. It was instrumented with 13 triaxial accelerometers distributed along equispaced sections of the blade.

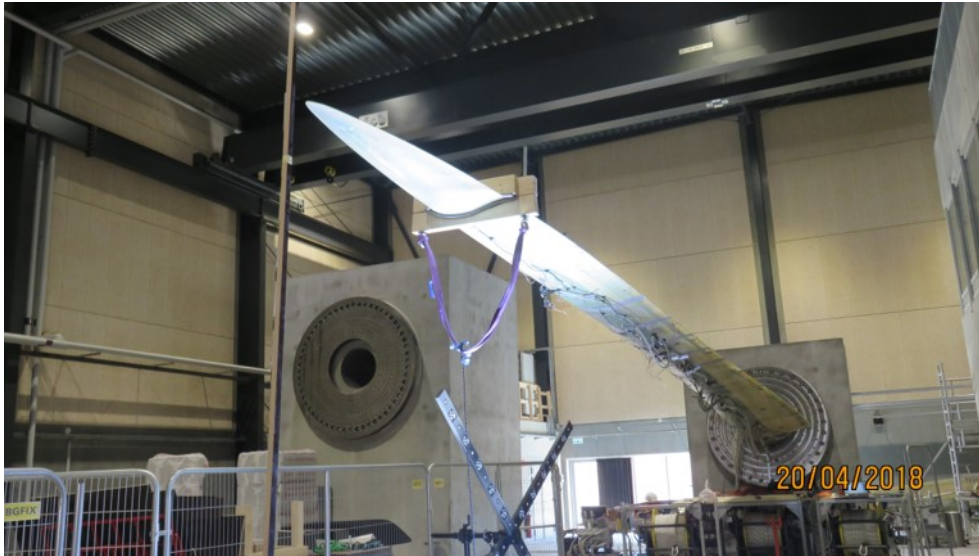


Figure 4.1.: Photo of the experimental setup of the pull and release tests

4.1.2. Data analysis

After choosing one reference location, time domain responses measured across the structure were used to calculate auto-correlation and cross-correlation functions.

Then, by taking the discrete Fourier transform of the correlation functions, autopowers and crosspowers spectra were obtained. Lastly, the crosspowers sum function was subjected to a curve-fit process, identical to the one used in EMA, in order to extract the modal parameters.

The analysis of the experimental data was carried out using the “Operational Modal Analysis” and the “Operational PolyMAX Modal Analysis” add-ins in Simcenter TestLab[®].

The first step in the analysis was the processing of the crosspowers and correlation functions from the time domain responses measured during the test. So, firstly, one response measurement location was designated as reference, in particular the chosen location was the accelerometer located in the center of the 11th section of the blade, and both the accelerations measured in x and y direction were considered as

references. Then it was possible to specify the number of time lags and the exponential window percentage to use in the processing of the functions. The number of time lags determines the frequency resolution of the crosspowers, which indeed is defined as:

$$\Delta f = \frac{F_s}{\text{number of time lags}} \quad (4.1)$$

where F_s is the sampling frequency of the data. This means that the higher is the number of time lags the finer is the frequency resolution. Anyway, finer frequency resolution results in reduced amplitude, so the crosspower functions get to be more spiky and this may complicate the curve-fitting process, so the number of time lags should be a balance between being able to separate closely spaced modes and having a clear crosspower function. [10] In this analysis the sampling frequency of the data was set to $100Hz$ and the number of time lags was set to 1024, resulting in a frequency resolution of $\simeq 0,01\%$. Another important setting, which has to be specified before being able to calculate the correlation and crosspower functions, is the exponential window percentage. This setting controls the exponential window applied to the correlation functions in order to reduce the effect of leakage, and the percentage value entered corresponds to the amplitude of the correlation function at the end of the time window. So the value chosen should be the one that makes the crosscorrelation function equal or close to zero by the end of the time window. In this analysis the exponential window percentage was set to 10%. The second step of the analysis consists in performing the curve-fitting process in order to extract the modal parameters of the structure. This was done in the same way as in the experimental modal analysis, that is selecting the stable poles in the stabilization diagram and then calculating the corresponding mode shapes. In this study the frequency bandwidth set for the analysis ranges from $0,10Hz$ to $50Hz$, and in the stabilization diagram it was possible to recognize only 5 different columns of stable poles, so 5 different modes. This is due to the fact that the crosspower functions obtained were very smooth, as it is possible to notice in this example of a crosspower sum taken from one of the tests:

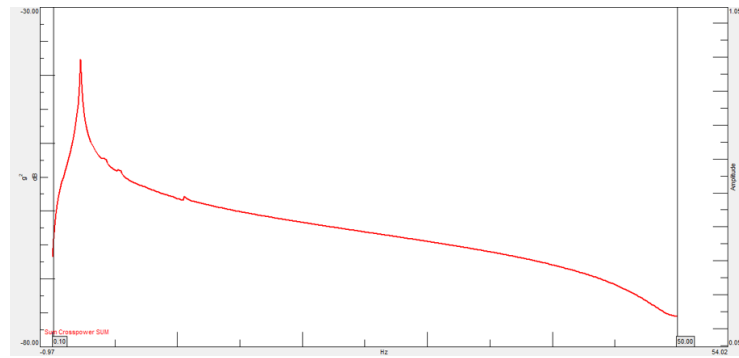


Figure 4.2.: Example of a Crosspower Sum obtained in one of the Pull & Release Test

The final step for OMA, as it is for EMA, is the model validation. Its aim is to verify if the operational modal model captures the modal characteristics of the system, by comparing the synthesized crosspowers to the measured ones. The modal model calculated in the previous step of the analysis can be said to be validated if the percentage of correlation is high, generally over $\simeq 95\%$, and so it was also in this case.

4.1.3. Results

These are the 4 mode sets obtained from the analysis of the pull and release tests performed after stopping the blade during its fatigue test at 4 different numbers of fatigue cycles:

Mode	$f_n(Hz)$	$\zeta_n(\%)$
1	2.251	0.463
2	4.222	0.414
3	5.365	0.64
4	9.242	0.507
5	10.488	0.749
(a) 4.5×10^5 cycles		

Mode	$f_n(Hz)$	$\zeta_n(\%)$
1	2.25	0.388
2	4.214	0.396
3	5.372	0.558
4	9.223	0.602
5	10.505	0.591
(b) 1.1×10^6 cycles		

Mode	$f_n(Hz)$	$\zeta_n(\%)$
1	2.247	0.422
2	4.212	0.532
3	5.366	0.563
4	9.225	0.63
5	10.499	0.549
(c) 1.5×10^6 cycles		

Mode	$f_n(Hz)$	$\zeta_n(\%)$
1	2.249	0.411
2	4.212	0.42
3	5.364	0.486
4	9.243	0.38
5	10.51	0.375
(d) 2×10^6 cycles		

Table 4.1.: Mode sets from Pull and Release test at 4.5×10^5 (a), 1.1×10^6 (b), 1.5×10^6 (c) and 2×10^6 (d) cycles

4.1. Pull and Release tests

After determining the mode sets, they have been compared to each other to see if there was some significant variation due to the fatigue damage. The result of the comparison between the natural frequencies and the damping is as follows:

Mode	$\Delta f_n\%$	$\Delta\zeta_n\%$	Mode	$\Delta f_n\%$	$\Delta\zeta_n\%$
1	0.044	16.415	1	0.089	9.021
2	0.189	4.348	2	0.047	34.343
3	0.130	12.969	3	0.112	0.896
4	0.206	18.540	4	0.022	4.817
5	0.172	20.961	5	0.057	7.276

(a) 4.5×10^5 & 1.1×10^6 cycles

Mode	$\Delta f_n\%$	$\Delta\zeta_n\%$
1	0.089	2.607
2	0.000	21.053
3	0.037	13.677
4	0.195	39.683
5	0.105	31.694

(b) 1.1×10^6 & 1.5×10^6 cycles

Mode	$\Delta f_n\%$	$\Delta\zeta_n\%$
1	0.089	2.607
2	0.000	21.053
3	0.037	13.677
4	0.195	39.683
5	0.105	31.694

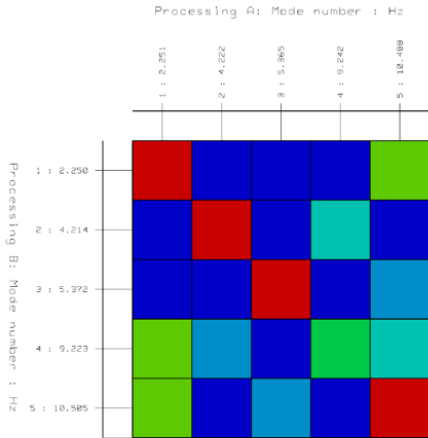
(c) 1.5×10^6 & 2×10^6 cycles

Table 4.2.: Frequency and Damping difference between P&R tests

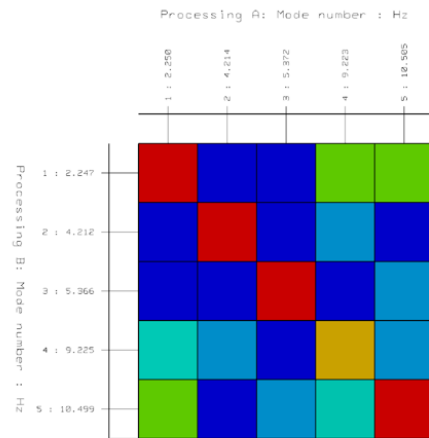
It can be seen that there are few differences between the natural frequencies, with a maximum of 0,2%, and there are more inconsistencies in the damping values, with differences that ranges from nearly 1% up to 40%.

Chapter 4. Modal analysis during fatigue test

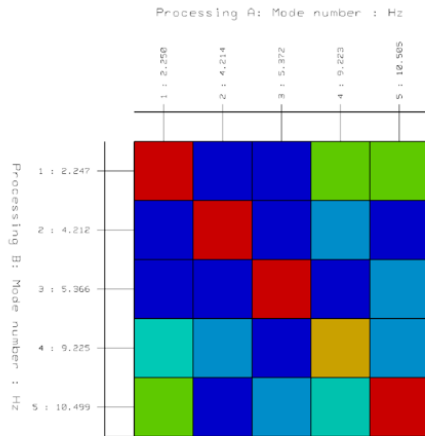
In addition to the comparison between the values of natural frequencies and damping, the MAC has also been calculated in order to compare the mode shapes. The resulting MAC matrices are as it follows:



(a) MAC between P&R tests at 4.5×10^5 and 1.1×10^6 cycles



(b) MAC between P&R tests at 1.1×10^6 and 1.5×10^6 cycles



(c) MAC between P&R tests at 1.5×10^6 and 2×10^6 cycles

Figure 4.3.: MAC matrices between the Pull and Release tests

4.2. Hammer tests

The hammer tests consisted in exciting the blade with a modal hammer and measuring its response with the same accelerometers used for the pull and release tests. Since in these tests we know the excitation, here it was possible to use the FRFs and to perform Experimental Modal Analysis.

4.2.1. Experimental setup

The experimental setup is the same as in the pull and release tests, so the blade was clamped to a rigid block through the circular interface plate in a flapwise configuration and it was instrumented with 13 triaxial accelerometers distributed along equispaced sections of the blade.

4.2.2. Data analysis and Results

The analysis of the experimental data was carried out using the “Modal Analysis” and the “PolyMAX Modal Analysis” add-ins in Simcenter TestLab[®].

The frequency bandwidth chosen for the analysis is equal to that used for the pull and release tests, so ranges from $0,10Hz$ to $50Hz$, nevertheless this time in the stabilization diagram it was possible to recognize a larger number of columns of stable poles, and the reason of this can be found in the much cleaner FRFs sum function obtained with respect to the crosspower sum functions obtained previously:

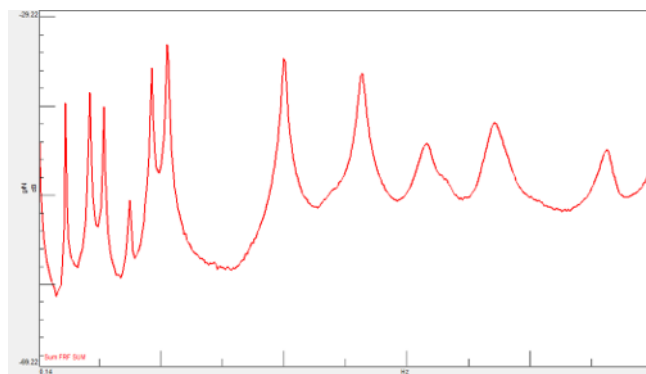


Figure 4.4.: Example of a FRFs Sum obtained in one of the Hammer Tests

In the first processing of these data it was chosen to select all the stable poles columns in the stabilization diagram within the selected frequency band. After that,

Chapter 4. Modal analysis during fatigue test

MLMM algorithm and Auto-MAC were calculated, to verify if the selected modes were actual modes of the blade. In particular in the first 3 tests were found 2 columns of stable modes more than in the last one. So, to figure out if these additional modes were actual modes of the blade, all the FRFs measured during the first three tests were analyzed to see if there was any peak at the frequencies of interest. This analysis resulted in the absence of any visible peak at those frequencies, and besides this, these modes, after the application of the MLMM algorithm, showed an high variation in the frequency and/or damping value. So it was decided to discard them in the second processing. In the following pictures we can see the stabilization diagrams and the FRFs of the first 3 tests, were it is highlighted the position of the discarded modes:

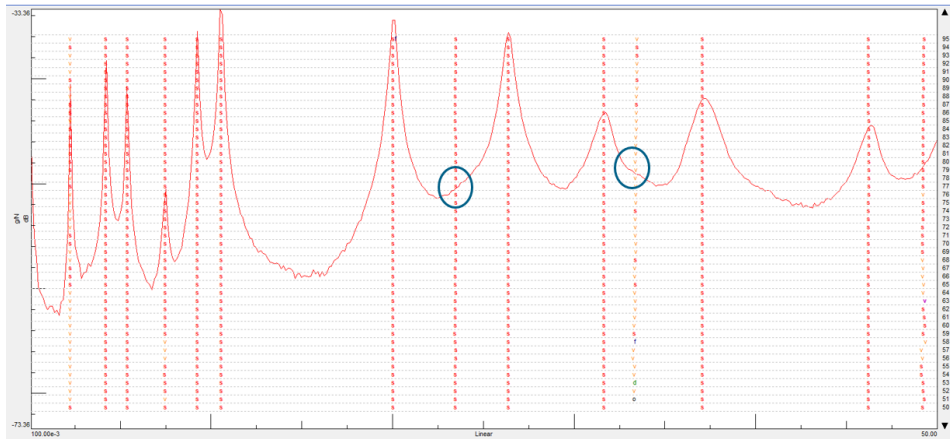


Figure 4.5.: Stabilization Diagram from the hammer test performed at 4.5×10^5 fatigue cycles

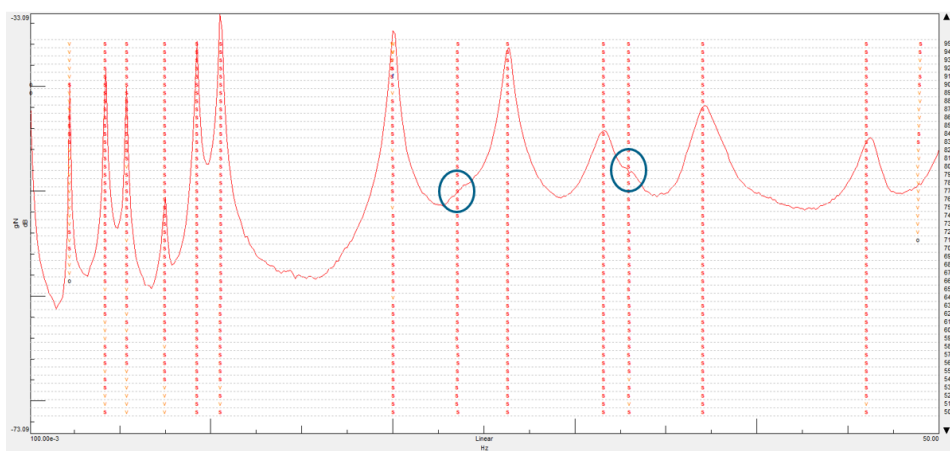


Figure 4.6.: Stabilization Diagram from the hammer test performed at 1.1×10^6 fatigue cycles

4.2. Hammer tests

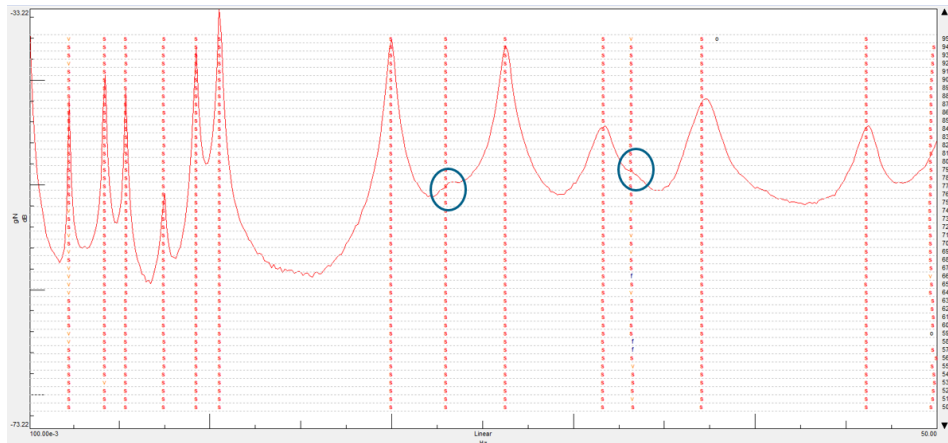
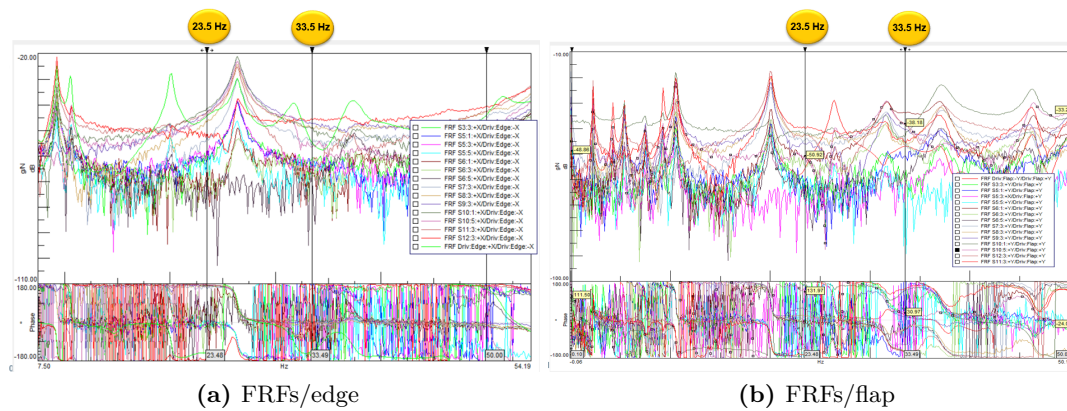


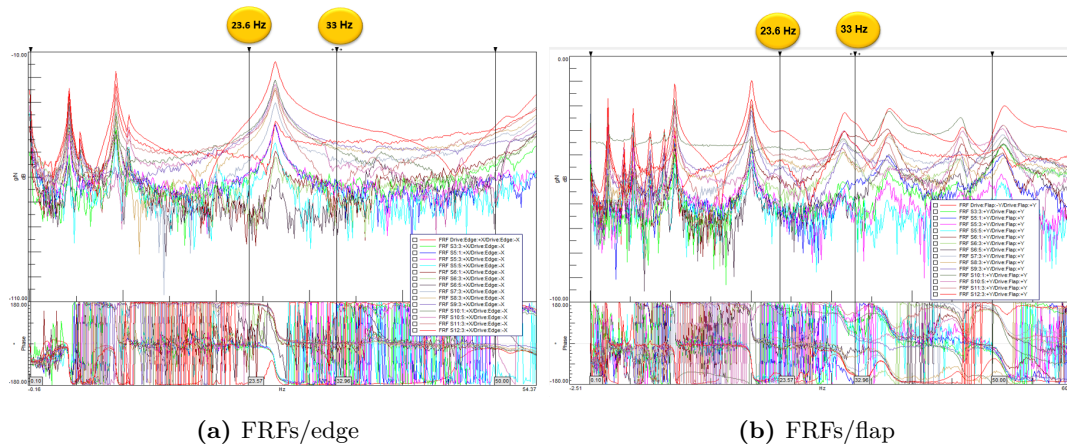
Figure 4.7.: Stabilization Diagram from the hammer test performed at 1.5×10^6 fatigue cycles



(a) FRFs/edge

(b) FRFs/flap

Figure 4.8.: FRFs at 4.5×10^5 fatigue cycles



(a) FRFs/edge

(b) FRFs/flap

Figure 4.9.: FRFs at 1.1×10^6 fatigue cycles

Chapter 4. Modal analysis during fatigue test

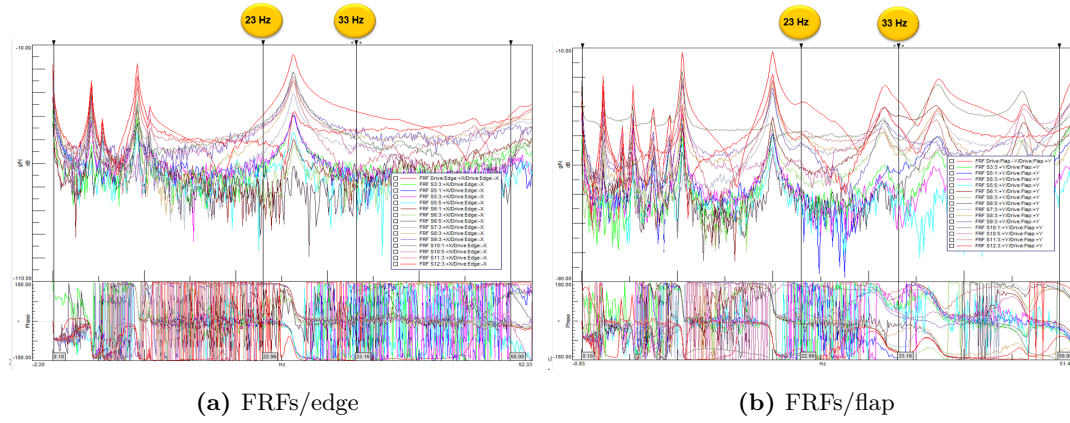


Figure 4.10.: FRFs at 1.5×10^6 fatigue cycles

In the second processing the following mode sets were obtained:

Mode	$f_n(Hz)$	$\zeta_n(\%)$
1	2.251	0.365
2	4.221	0.339
3	5.39	0.413
4	7.471	0.772
5	9.243	0.416
6	10.552	0.344
7	20.044	0.761
8	26.38	0.906
9	31.65	1.732
10	37.077	1.79
11	46.236	1.09

(a) 4.5×10^5 cycles

Mode	$f_n(Hz)$	$\zeta_n(\%)$
1	2.256	0.27
2	4.221	0.31
3	5.389	0.252
4	7.476	0.943
5	9.242	0.434
6	10.554	0.374
7	20.009	0.724
8	26.332	0.883
9	31.583	1.807
10	37.048	1.85
11	46.024	1.19

(b) 1.1×10^6 cycles

Mode	$f_n(Hz)$	$\zeta_n(\%)$
1	2.243	0.301
2	4.214	0.286
3	5.38	0.339
4	7.466	0.967
5	9.237	0.448
6	10.538	0.332
7	19.963	0.81
8	26.268	0.93
9	31.635	1.88
10	37.068	1.881
11	46.112	1.167

(c) 1.5×10^6 cycles

Mode	$f_n(Hz)$	$\zeta_n(\%)$
1	2.956	0.943
2	4.213	0.325
3	5.383	0.311
4	7.448	0.94
5	9.249	0.485
6	10.526	0.303
7	19.465	1.855
	21.256	2.076
8	26.181	0.926
9	31.513	2.213
10	36.966	1.529
11	46.144	1.152

(d) 2×10^6 cycles

Table 4.3.: Mode sets obtained from the hammer tests at 4.5×10^5 (a), 1.1×10^6 (b), 1.5×10^6 (c) and 2×10^6 (d) cycles

We can notice that in the 4th mode set there is one more mode than in the others, and it was added in the same row of mode 7 because it seems like if the 7th mode splitted in two in the last test. This assumption arised firstly after observing the overlay of the FRFs sum functions from the 4 tests:

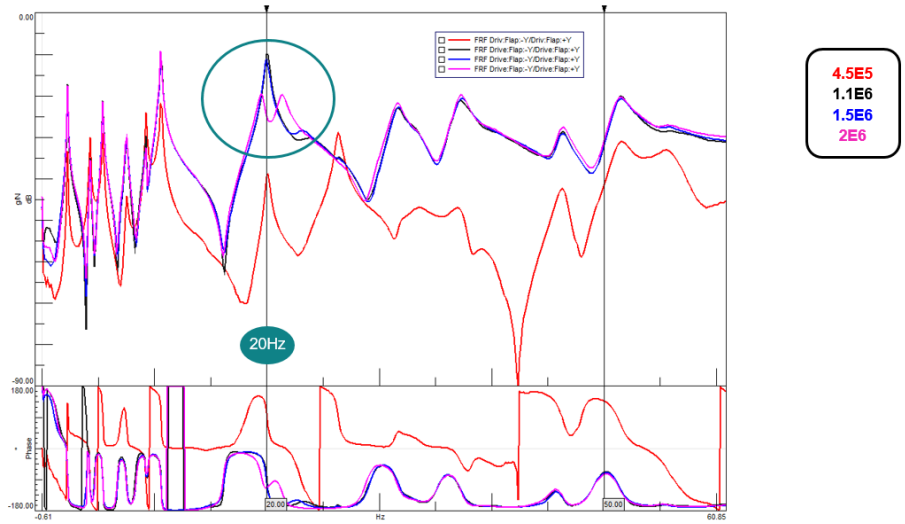


Figure 4.11.: Overlay of the FRF Sum functions coming from the 4 hammer tests

Moreover this supposition seems to be in agreement also with the results of the MAC matrices calculated between the different tests:

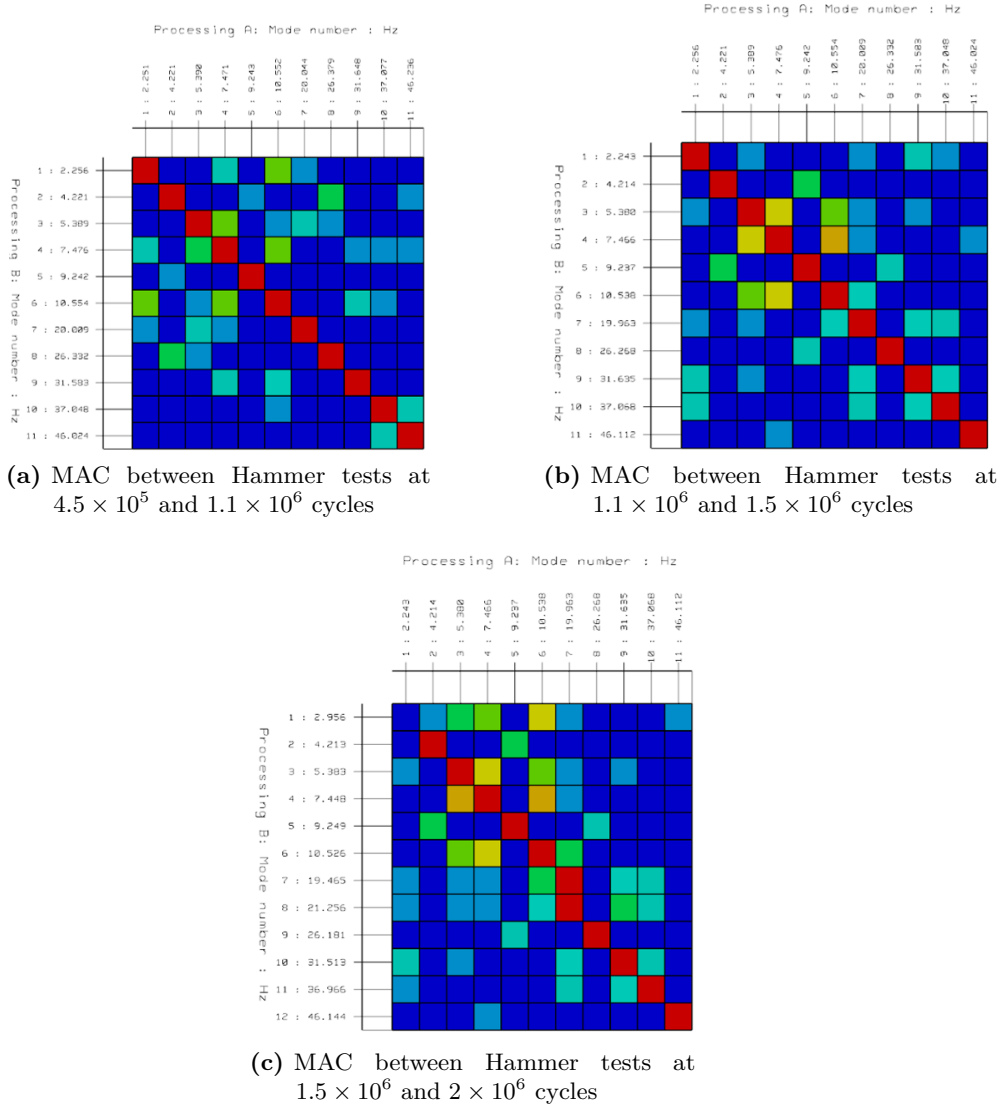


Figure 4.12.: MAC matrices between the Hammer tests

In fact we can notice that the rows of the 3rd matrix corresponding to the 7th and 8th mode of the 4th test are equal to each other. This sort of "splitting" of the seventh mode could be considered as an effect of the fatigue damage on the blade. Beside this, as for the pull and release tests, it was determined the percentage difference between the frequency and damping values of the 4 mode sets, but like in the previous case we can't notice any significant change, except for the last test:

Mode	$\Delta f_n\%$	$\Delta\zeta_n\%$	Mode	$\Delta f_n\%$	$\Delta\zeta_n\%$
1	0.222	26.027	1	0.576	11.481
2	0.000	8.555	2	0.166	7.742
3	0.019	38.983	3	0.167	34.524
4	0.067	22.150	4	0.134	2.545
5	0.011	4.327	5	0.054	3.226
6	0.019	8.721	6	0.152	11.230
7	0.175	4.862	7	0.230	11.878
8	0.178	2.539	8	0.243	5.323
9	0.205	4.330	9	0.165	4.040
10	0.078	3.352	10	0.054	1.676
11	0.459	9.174	11	0.191	1.933
			11	0.459	9.174

(a) 4.5×10^5 & 1.1×10^6 cycles

(b) 1.1×10^6 & 1.5×10^6 cycles

Mode	$\Delta f_n\%$	$\Delta\zeta_n\%$
1	31.788	213.289
2	0.024	13.636
3	0.056	8.260
4	0.241	2.792
5	0.130	8.259
6	0.114	8.735
7	2.495	129.012
	6.477	156.296
8	0.331	0.430
9	0.386	17.713
10	0.275	18.713
11	0.069	1.285

(c) 1.5×10^6 & 2×10^6 cycles

Table 4.4.: Frequency and Damping difference between Hammer tests

Chapter 5.

Structural dynamic analysis on the undamaged blade

This chapter deals with the structural dynamic analysis of the undamaged blade. It consists in four main steps:

- Experimental modal analysis;
- Finite element analysis;
- Correlation between experimental and simulation results;
- Model updating.

5.1. Experimental modal analysis

5.1.1. Experimental setup

The test blade was supported with two elastic chords in the edgewise direction to provide free-free boundary conditions (Figure 5.1). It has been simultaneously excited in the flapwise and edgewise directions with two electrodynamic shakers. The blade was instrumented with 15 accelerometers placed along the blade at 1m distance from each other (Figure 5.2). Additionally each station was measured in 8 locations (Figure 5.3). So the test was carried out using the roving accelerometer technique, meaning that in each run one accelerometer was placed in each section aligned to the others, all placed in the same station of the section. Therefore the total number of runs was 8.

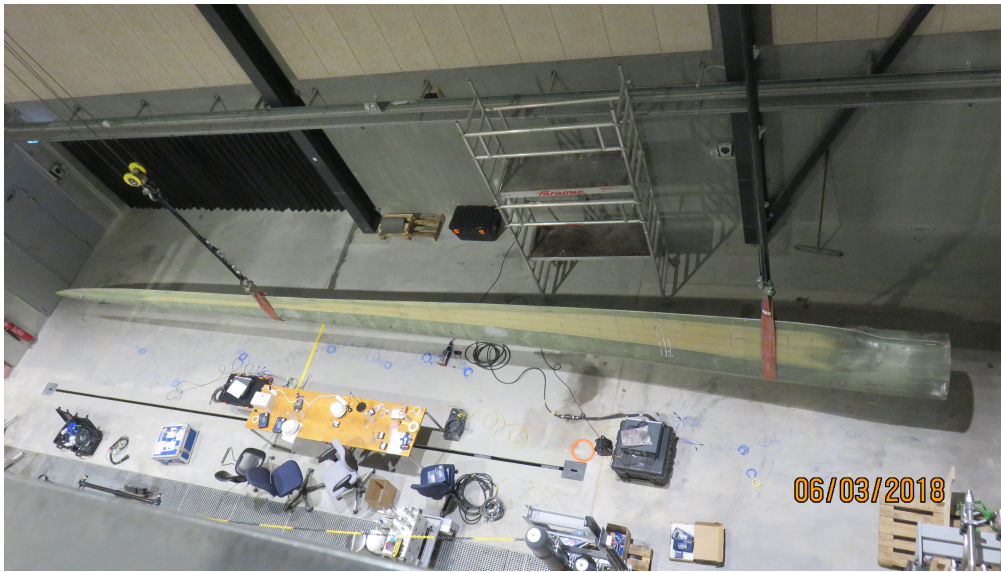


Figure 5.1.: Instrumented blade on the test stand in the free-free support configuration

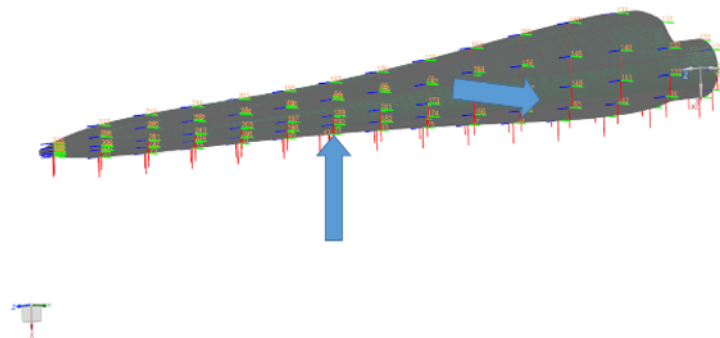


Figure 5.2.: Excitation points and sensors

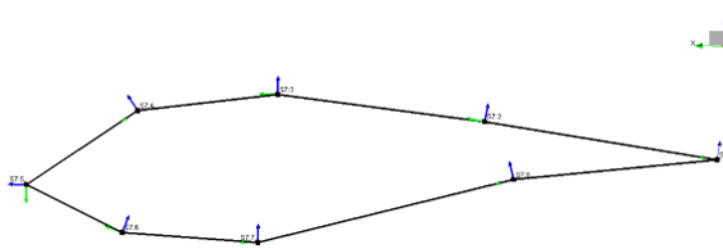


Figure 5.3.: Sensors placed in each station

5.1.2. Data analysis and Results

The analysis of the experimental data was carried out using the “Modal Analysis”, “PolyMAX Modal Analysis” and ”MLMM” add-ins in Simcenter TestLab® . The frequency band chosen for the analysis ranges from 0,1 to 102Hz, and this is the corresponding stabilization chart obtained with the Polymax algorithm:

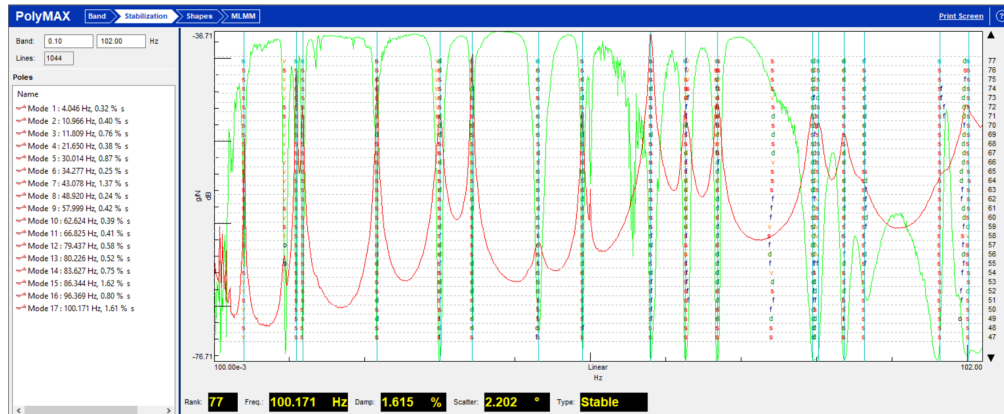
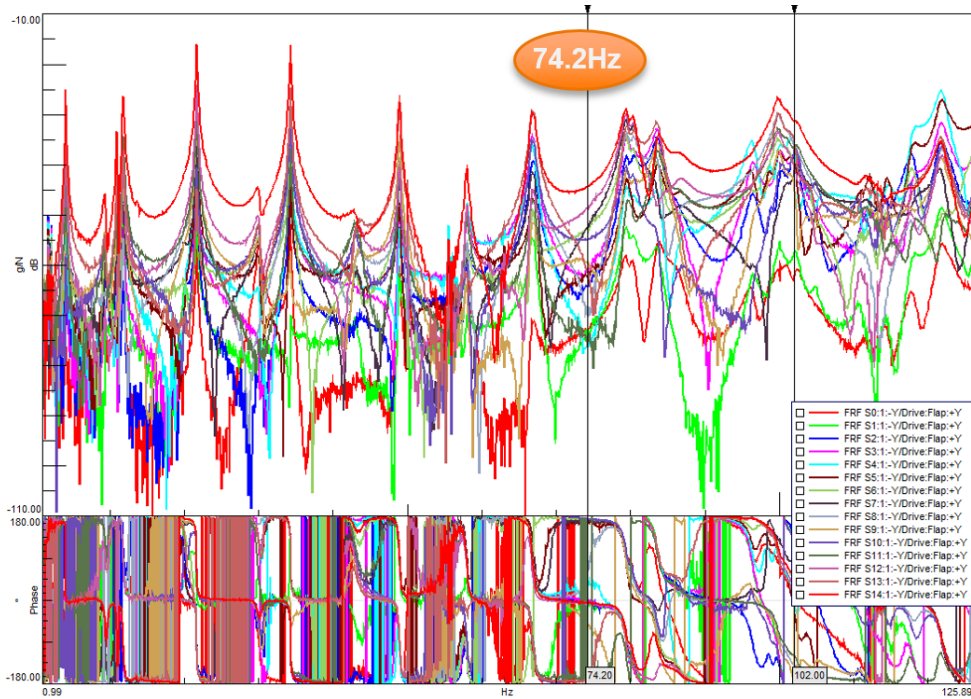
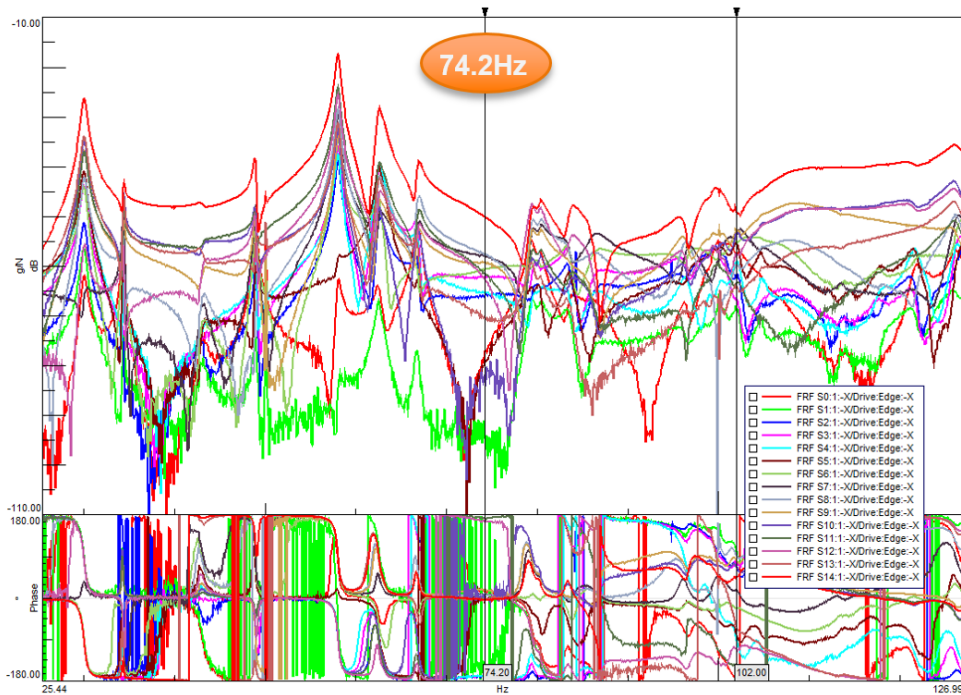


Figure 5.4.: Stabilization chart obtained with Polymax algorithm in the chosen frequency-band

It can be noticed that there are 19 columns of poles in the selected frequency band, but despite that only 17 of them were included in the final set at the end of the study. The first exclusion concerns the mode with a natural frequency equal to 74.2Hz, and resulted from the application of the MLMM (Maximum Likelihood Modal Model) algorithm. In particular, after 150 iterations of MLMM, the natural frequency of this mode increased by 5Hz, becoming 79.3Hz. So further analysis have been made in order to understand the reasons behind this result; in particular all the FRFs from the same run, so from the same station in each section, were collected and overlapped to see if there was any spike at the frequency of 74Hz.



(a) FRFs from Station 1: -Y/DriveFlap:+Y



(b) FRFs from Station 1: -X/DriveFlap:+X

Figure 5.5.: FRFs from Station 1

5.1. Experimental modal analysis

After proving that there were no peaks at the frequency of interest, this mode was excluded from the subsequent analyses. The second exclusion concerns the mode with a natural frequency equal to 9.4Hz, and it is related to the correlation between simulation and experimental results, so it will be detailed in the following paragraphs. Anyway this is the final mode set obtained from the experimental analysis after these 2 exclusions:

Mode	Frequency (Hz)	Damping (%)
Mode 1	4.042	0.46
Mode 2	10.966	0.412
Mode 3	11.813	0.761
Mode 4	21.654	0.406
Mode 5	29.996	0.975
Mode 6	34.285	0.245
Mode 7	43.139	1.37
Mode 8	48.927	0.288
Mode 9	58.009	0.41
Mode 10	62.637	0.586
Mode 11	66.826	0.461
Mode 12	79.424	0.588
Mode 13	80.265	0.582
Mode 14	83.723	0.735
Mode 15	85.783	1.457
Mode 16	96.134	0.832
Mode 17	100.266	1.212

Table 5.1.: Final mode set from the EMA on the undamaged blade

5.2. Finite element analysis

The model was originally generated by using the commercial software MSC Patran[®] and DTU Wind Energy in-house software Blade Modeling Tool (BMT). Then it was imported in Simcenter 3D[®] and was solved using "SOL 103 Real Eigenvalues". The model is discretized with approximately 130.000 layered 20-noded continuum elements (CHEXA), and the composite layup consists of 6 to 32 plies through the thickness.

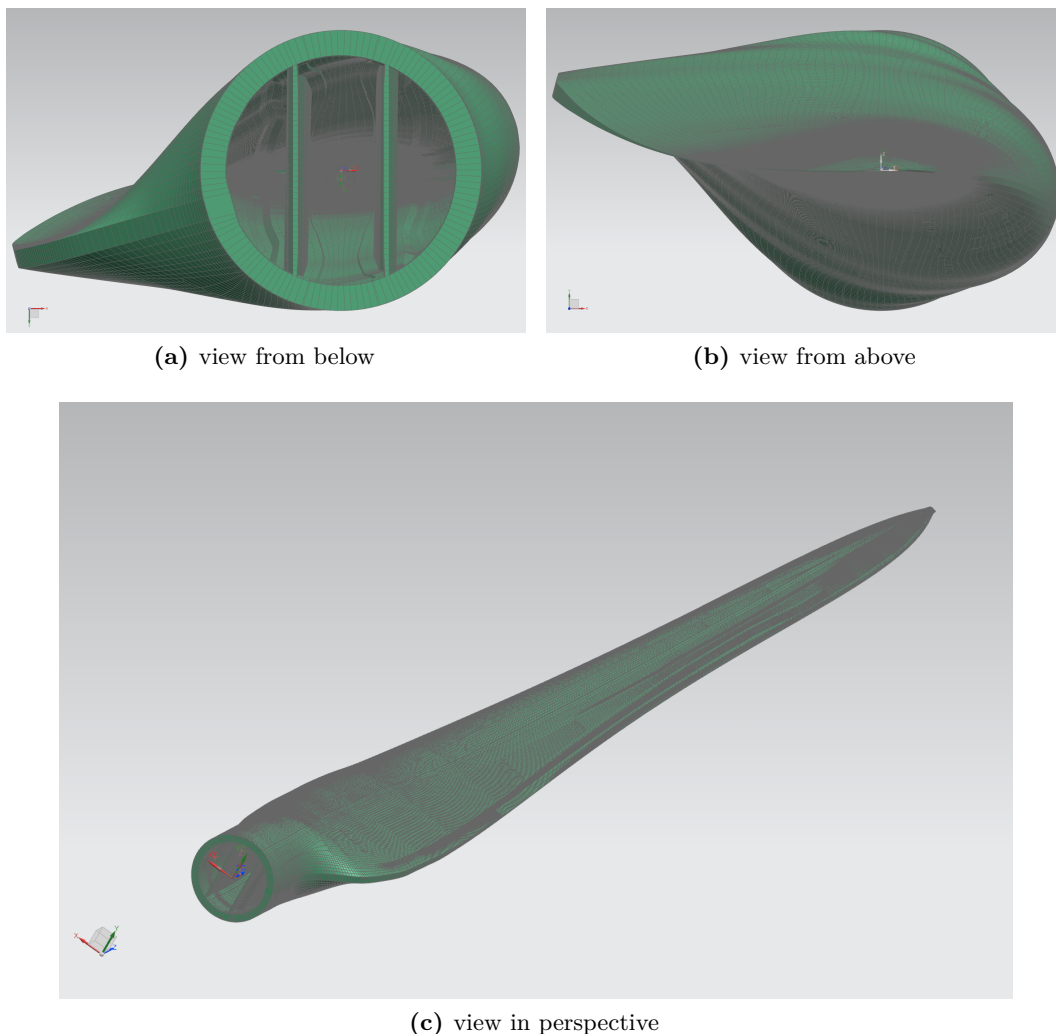


Figure 5.6.: Finite element model of the blade in Simcenter3D[®]

Then it is important to underline that since the blade manufacturer had not stated the exact properties for the fibers and matrix material, properties from comparable materials described in literature have been used:

Mechanical properties	UNIAX	BIAX	TRIAX	Chop	Core	Glue	Gelcoat
E1 [MPa]	37800	9550	18700	13600	48.5	3009	2000
E2 [MPa]	11100	9550	10900	13600			
G12 [MPa]	3270	10100	7720	5130			
ν_{12}	0.24	0.62	0.55	0.32	0.4	0.3	0.3
ρ [kg/m ³]	1850	1780	1780	1684	80	1540	1500
Thickness [mm]	0.95	0.5	0.75	0.3	5-10	-	0.6
Design strength (PSF 2.205)							
X_T [MPa]	360.0	69.3	186.0	56.2	x	x	x
X_C [MPa]	257.0	64.9	152.0	56.2	x	x	x
Y_T [MPa]	24.8	69.3	30.5	56.2	x	x	x
Y_C [MPa]	63.5	64.9	51.5	56.2	x	x	x
S [MPa]	16.6	55.9	42.3	23.9	x	x	x

Figure 5.7.: Values of the properties of the materials used in the model

This could be the reason of a non-optimal correlation between the simulation and experimental results and this is why the model updating was carried out focusing on the changing of the material properties.

5.3. Correlation between experimental and simulation results

The correlation between experimental and simulation results was carried out on Simcenter 3D[®] after importing the universal file of the experimental results from Simcenter TestLab[®]. This is the MAC matrix coming from the first correlation:

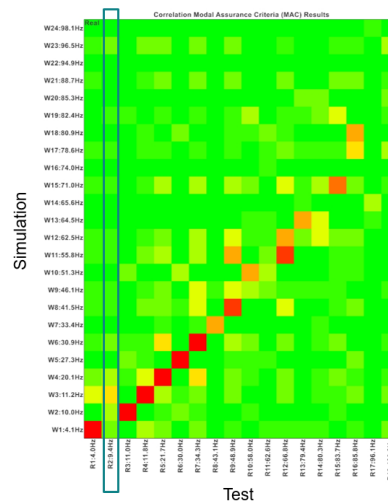


Figure 5.8.: MAC matrix from the 1st correlation

It can be noticed that the correlation of the 2nd experimental mode with the simulation modes is always low, so this means that the mode is not present in the simulation. This is why this mode was excluded from the experimental mode set, so this is the reason why the final mode set obtained from the experimental modal analysis consists of 17 modes.

Then, since the diagonal values of the MAC matrix were not high enough, the COMAC has also been analyzed, to see which sensor had a negative influence on the MAC matrix of the correlation. In particular the sensors where the COMAC is low are the sensors at which the individual MAC components are poorest. Thanks to the COMAC analysis it was noticed that the sensors placed on the leading edge of the blade were problematic, so they were removed to see the variation in the correlation MAC. And since after their removal the MAC improved substantially, it was decided to exclude them from the subsequent analyses.

5.3. Correlation between experimental and simulation results

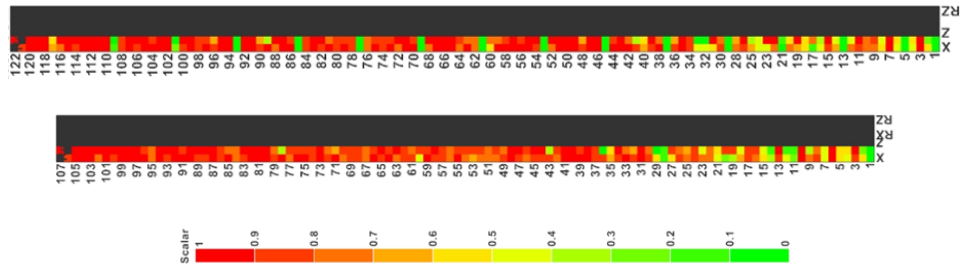


Figure 5.9.: COMAC graphs before and after removing problematic sensors

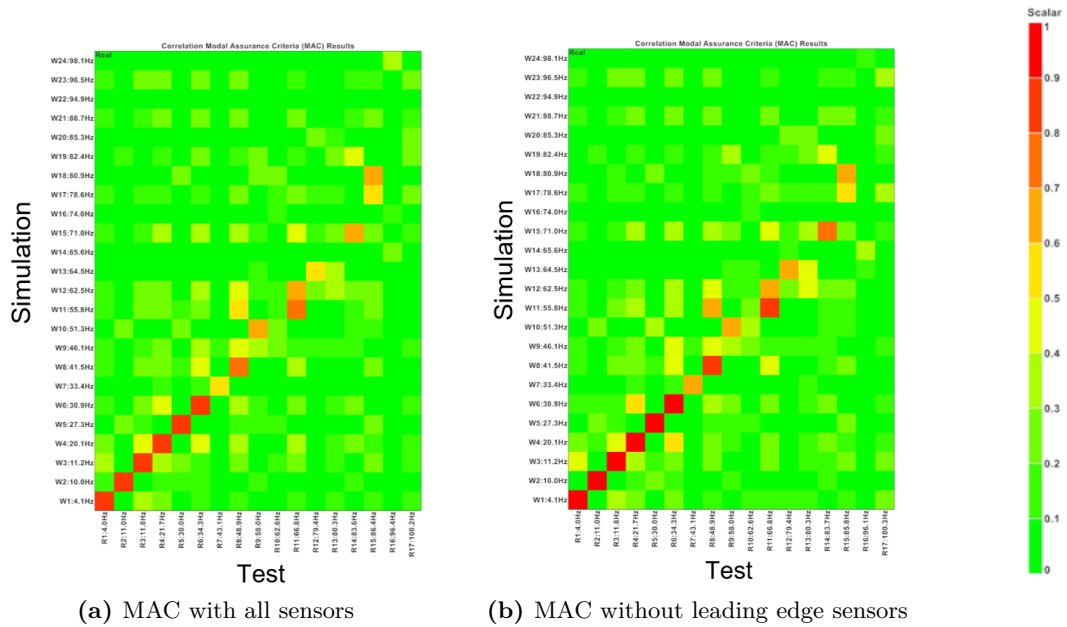


Figure 5.10.: MAC graphs before (a) and after (b) removing problematic sensors

Test Mode	Test Frequency (Hz)	Simulation Mode	Simulation Frequency (Hz)	MAC
1	4,04	1	4,12	0,85
2	10,97	2	10,03	0,84
3	11,81	3	11,22	0,87
4	21,66	4	20,12	0,88
5	30,00	5	27,30	0,85
6	34,28	6	30,88	0,82
7	43,09	7	33,42	0,52
8	48,93	8	41,47	0,75
9	58,01	10	51,28	0,65
11	66,82	11	55,81	0,73
12	79,43	13	64,51	0,51
14	83,64	15	71,00	0,61
15	86,36	18	80,87	0,62

(a) Some of the MAC diagonal values before removing leading edge sensors

Test Mode	Test Frequency (Hz)	Simulation Mode	Simulation Frequency (Hz)	MAC
1	4,04	1	4,12	0,96
2	10,97	2	10,03	0,96
3	11,81	3	11,22	0,97
4	21,65	4	20,12	0,96
5	30,00	5	27,30	0,96
6	34,29	6	30,88	0,90
7	43,14	7	33,42	0,60
8	48,93	8	41,47	0,82
9	58,01	10	51,28	0,68
11	66,83	11	55,81	0,82
12	79,43	13	64,51	0,62
14	83,73	15	71,00	0,71
15	85,79	18	80,87	0,64

(b) Some of the MAC diagonal values after removing leading edge sensors

Test Mode	Simulation Mode	Δ MAC	Δ MAC%
1	1	0,105	12,303
2	2	0,119	14,199
3	3	0,092	10,496
4	4	0,087	9,935
5	5	0,106	12,486
6	6	0,076	9,246
7	7	0,081	15,503
8	8	0,080	10,678
9	10	0,033	5,047
11	11	0,090	12,245
12	13	0,109	21,412
14	15	0,102	16,831
15	18	0,012	1,991

(c) MAC variation

Table 5.2.: MAC values before and after removing problematic sensors

5.4. Model updating

The Model Updating aimed at improving the correlation between experimental and simulation results by modifying the finite element model of the blade. It consisted in performing two parameter optimizations using the software HEEDS[®], and as objectives of the optimizations it was chosen to:

1. minimize the differences between the natural frequencies of the simulation and of the experimental data;
2. maximize the MAC between test and simulation.

In particular:

- in the first optimization only objective 1 has been taken into account;
- in the second one both objectives have been chosen.

And it is important to underline that only the pairs of modes with an high value of MAC were considered in this optimization:

Test Mode	Simulation Mode
1	1
2	2
3	3
4	4
5	5
6	6
7	7
8	8
9	10
11	11
12	13
14	15
15	18

As design variables the following material properties have been chosen: density and Young's Modulus of TRIAX, BIAx and UNIAX materials, with a range of $\pm 10\%$ with respect to their baseline value.

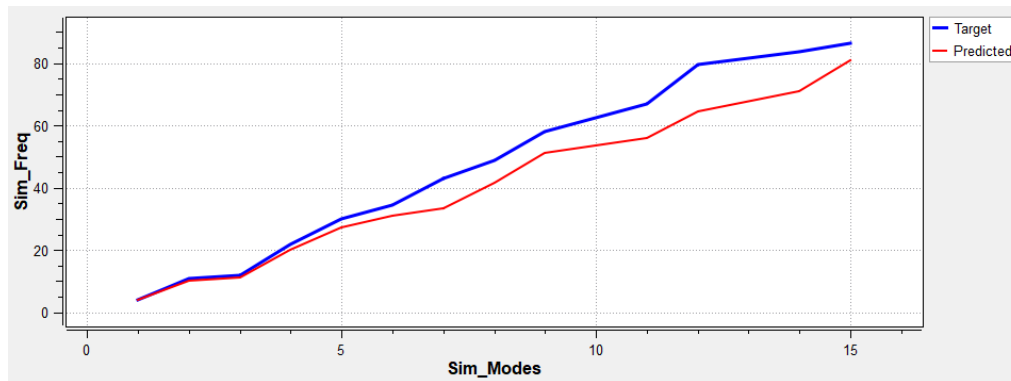
5.4.1. First optimization

In this case the only objective of the algorithm was to minimize the differences between the natural frequencies of the simulation and of the experimental results, and it has been translated into the minimization of the Root Medium Square Error

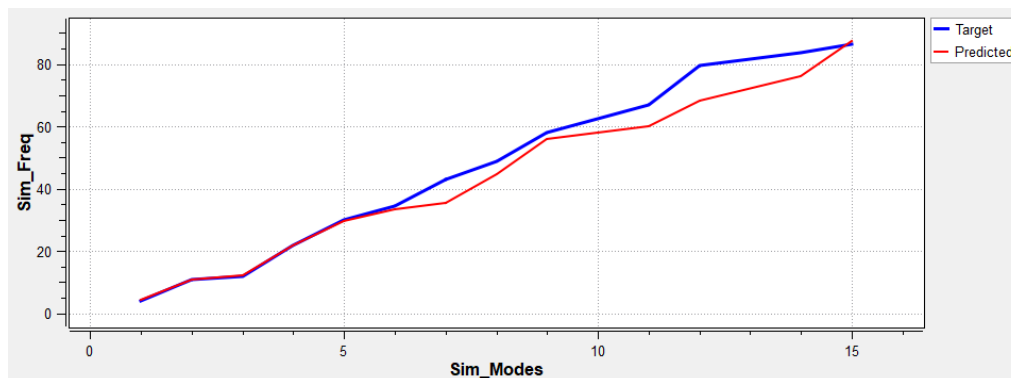
(RMSE) between two lines:

- the one define by the test's natural frequencies,
- and the one defined by the simulation's natural frequencies.

These graphs represent respectively the starting point before the optimization and the best design found in the optimization:



(a) Frequency difference before optimization



(b) Frequency difference in the best design found in the optimization

Figure 5.11.: Frequency difference before (a) and after (b) 1st optimization

Where the blue line represents the natural frequencies obtained from the analysis of the experimental data, while the red one represents the natural frequencies obtained in the simulation. So by simply looking at these graphs we notice that the difference between the natural frequencies of the two sets of modes has been reduced thanks to the optimization, then if we look at the numerical values we realize that the frequency difference has been reduced in all pairs of modes, made exception for the first one:

F_{test} (Hz)	$F_{sim,i}$ (Hz)	$F_{sim,f}$ (Hz)	ΔF_i (Hz)	ΔF_f (Hz)	$\frac{\Delta F_f - \Delta F_i}{\Delta F_i} * 100(\%)$
4,04	4,12	4,51	0,08	0,47	487,50
10,97	10,03	10,98	0,94	0,01	-98,94
11,81	11,22	12,25	0,59	0,44	-25,42
21,66	20,12	21,89	1,54	0,23	-85,06
30,00	27,30	29,79	2,7	0,21	-92,22
34,28	30,88	33,30	3,4	0,98	-71,18
43,09	33,42	35,42	9,67	7,67	-20,68
48,93	41,47	44,56	7,46	4,37	-41,42
58,01	51,28	55,82	6,73	2,19	-67,46
66,82	55,81	60,04	11,01	6,78	-38,42
79,42	64,51	68,35	14,91	11,07	-25,75
83,64	71,00	76,23	12,64	7,41	-41,38
86,35	80,87	87,36	5,48	1,01	-81,57

Table 5.3.: Frequency difference before and after 1st optimization

Where F_{test} are the natural frequencies from the experimental data, $F_{sim,i}$ are the natural frequencies from the simulation before the optimization, $F_{sim,f}$ are the natural frequencies from the simulation corresponding to the best design found in the optimization, ΔF_i and ΔF_f are defined as $\Delta F_i = |F_{test} - F_{sim,i}|$, $\Delta F_f = |F_{test} - F_{sim,f}|$.

But if we consider the variation of the MAC caused by the optimization, we notice that in most of the pairs of modes the MAC has decreased:

MAC_i	MAC_f	ΔMAC	$\frac{MAC_f - MAC_i}{MAC_i} * 100$
0.956	0.956	0.0001	0.006
0.959	0.958	-0.001	-0.143
0.967	0.967	0.00002	0.002
0.964	0.963	-0.0005	-0.051
0.959	0.953	-0.006	-0.676
0.904	0.808	-0.095	-11.792
0.628	0.550	-0.078	-14.196
0.828	0.799	-0.029	-3.648
0.692	0.722	0.030	4.164
0.841	0.824	-0.017	-2.064
0.630	0.548	-0.082	-14.976
0.729	0.704	-0.024	-3.475
0.706	0.746	0.040	5.387

Table 5.4.: MAC variation after 1st optimization

Then, observing the values of the design variables in the best design found by the

optimization, and comparing them with their range of variation and their baseline values, we notice that the densities of all 3 materials considered are minimized while the Young's Modulus are maximized. This is due to the fact that the simulation's natural frequencies are originally lower than the test's ones, so the algorithm tries to increase the simulation's frequencies by increasing the stiffness of the model.

Design Variable	Baseline value	Lower bound	Upper bound	Best value	Correlation Best value/Range
ρ_T [kg/mm ³]	1,78E-06	1,61E-06	1,96E-06	1,61E-06	min
E_{1T} [kPa]	1,87e7	1,68E+07	2,05E+07	2,05E+07	max
E_{2T} [kPa]	1,09E+07	9,85E+06	1,20E+07	1,20E+07	max
E_{3T} [kPa]	9,62E+06	8,66E+06	1,06E+07	1,06E+07	max
ρ_U [kg/mm ³]	1,85E-06	1,66E-06	2,03E-06	1,66E-06	min
E_{1U} [kPa]	3,78E+07	3,40E+07	4,16E+07	4,16E+07	max
E_{2U} [kPa]	1,11E+07	9,95E+06	1,22E+07	1,22E+07	max
E_{3U} [kPa]	9,87E+06	8,89E+06	1,09E+07	1,09E+07	max
ρ_B [kg/mm ³]	1,78E-06	1,69E-06	1,87E-06	1,69E-06	min
E_{1B} [kPa]	9,55E+06	8,59E+06	1,05E+07	1,05E+07	max
E_{2B} [kPa]	9,55E+06	8,59E+06	1,05E+07	1,05E+07	max
E_{3B} [kPa]	9,83E+06	8,84E+06	1,08E+07	1,08E+07	max

Table 5.5.: Values of the design variables before and after 1st optimization

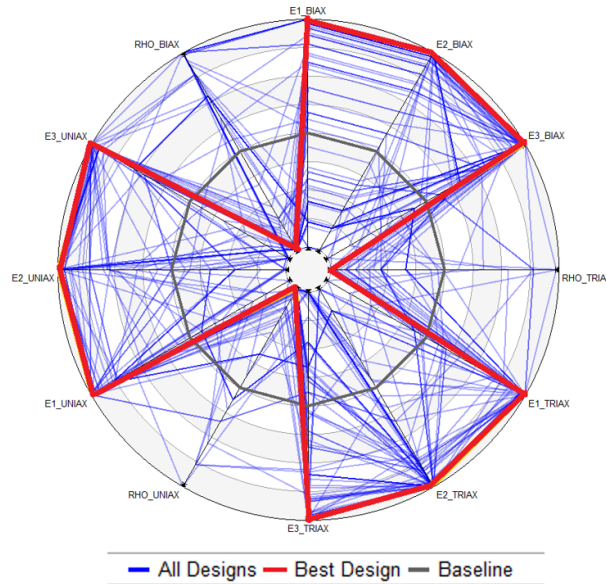
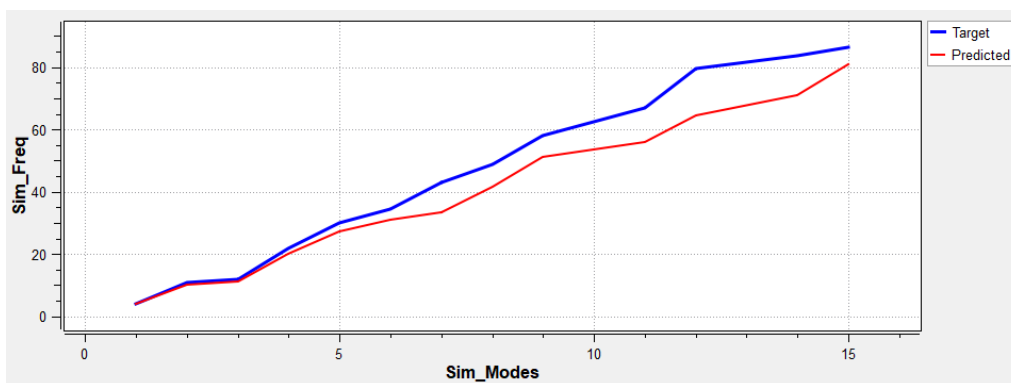


Figure 5.12.: Graph of the design variables values in all designs of the 1st optimization

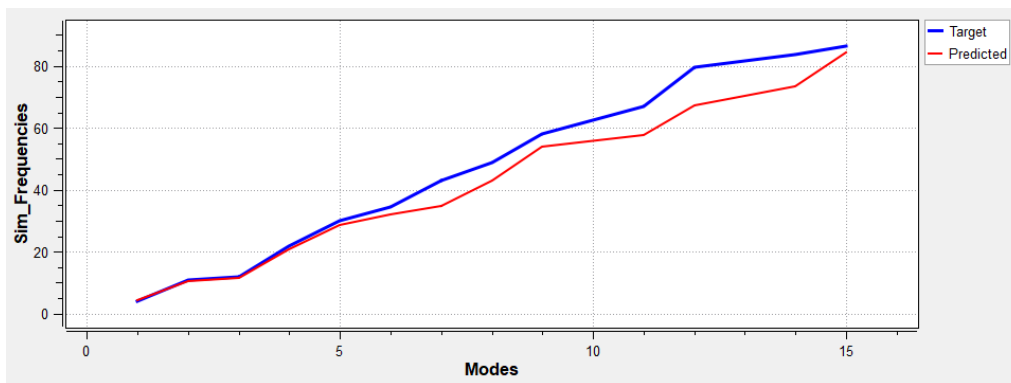
5.4.2. Second optimization

The second optimization is equal to the first one regarding the first objective, but in addition, it has the further objectives of maximization of the MAC values. In particular, the maximization of the MAC values has been added as multiple objectives, because each MAC had to be calculated separately after importing the modal vectors from the Simcenter Testlab's universal file and Simcenter 3D.

These are the results obtained with this second optimization as regards the natural frequencies and the MAC values:



(a) Frequency difference before optimization



(b) Frequency difference in the best design found in the optimization

Figure 5.13.: Frequency difference before (a) and after (b) 2nd optimization

F_{test} (Hz)	$F_{sim,i}$ (Hz)	$F_{sim,f}$ (Hz)	ΔF_i (Hz)	ΔF_f (Hz)	$\frac{\Delta F_f - \Delta F_i}{\Delta F_i} * 100(\%)$
4,04	4,12	4,25	0,08	0,20	-160,60
10,97	10,03	10,50	0,94	0,47	50,24
11,81	11,22	11,62	0,59	0,20	66,66
21,65	20,12	20,82	1,53	0,84	45,45
30,00	27,3	28,66	2,70	1,33	50,59
34,29	30,88	32,07	3,41	2,22	34,88
43,14	33,42	34,83	9,72	8,32	14,46
48,93	41,47	43,08	7,46	5,85	21,61
58,01	51,28	53,92	6,73	4,09	39,20
66,83	55,81	57,82	11,02	9,00	18,26
79,43	64,51	67,17	14,92	12,26	17,80
83,73	71	73,53	12,73	10,20	19,87
85,79	80,87	84,21	4,92	1,58	67,80

Table 5.6.: Frequency difference before and after 2nd optimization

MAC_i	MAC_f	ΔMAC	$\frac{MAC_f - MAC_i}{MAC_i} * 100$
0,956	0,956	0,0001	0,009
0,958	0,947	-0,011	-1,175
0,966	0,966	0,000	-0,018
0,963	0,963	0,000	0,015
0,959	0,954	-0,004	-0,439
0,901	0,909	0,009	0,951
0,603	0,616	0,013	2,137
0,825	0,835	0,010	1,230
0,682	0,702	0,020	2,962
0,823	0,813	-0,011	-1,290
0,619	0,669	0,050	8,081
0,707	0,708	0,001	0,106
0,637	0,708	0,071	11,125

Table 5.7.: MAC variation after 2nd optimization

So we can notice that in this case, besides having a reduction of the difference between experimental and simulation natural frequencies as in the first optimization, we have a greater improvement of the MAC values. Then, if we look at the values of the design variables in the best design, and we compare them with their range of variation and their baseline values, we can notice that there isn't the same trend as before, because the variables assume also intermediate values in their range.

Design Variable	Baseline value	Lower bound	Upper bound	Best value	Correlation Best value/Range
ρ_T [kg/mm ³]	1,78E-06	1,61E-06	1,96E-06	1.61E-06	min
E_{1T} [kPa]	1,87E+07	1,68E+07	2,05E+07	1.96E+07	
E_{2T} [kPa]	1,09E+07	9,85E+06	1,20E+07	1.04E+07	
E_{3T} [kPa]	9,62E+06	8,66E+06	1,06E+07	8.91E+06	
ρ_U [kg/mm ³]	1,85E-06	1,66E-06	2,03E-06	1.66E-06	min
E_{1U} [kPa]	3,78E+07	3,40E+07	4,16E+07	3.69E+07	
E_{2U} [kPa]	1,11E+07	9,95E+06	1,22E+07	1.18E+07	
E_{3U} [kPa]	9,87E+06	8,89E+06	1,09E+07	8.89E+06	min
ρ_B [kg/mm ³]	1,78E-06	1,69E-06	1,87E-06	1.95E-06	max
E_{1B} [kPa]	9,55E+06	8,59E+06	1,05E+07	8.72E+06	
E_{2B} [kPa]	9,55E+06	8,59E+06	1,05E+07	8.72E+06	
E_{3B} [kPa]	9,83E+06	8,84E+06	1,08E+07	1.08E+07	

Table 5.8.: Values of the design variables before and after 1st optimization

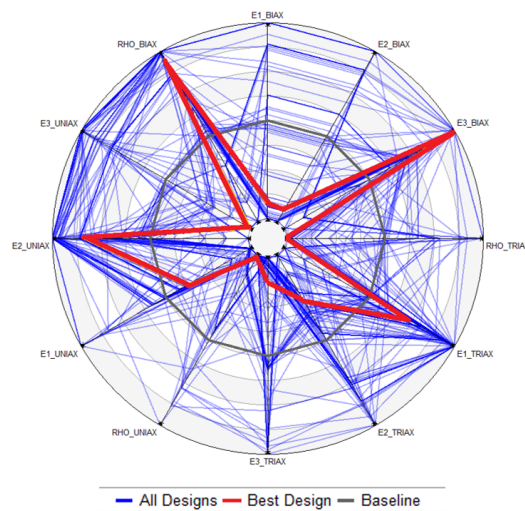


Figure 5.14.: Graph of the design variables values in all designs of the 2nd optimization

Chapter 6.

Conclusions and future works

In conclusion we can say that, regarding the results obtained from the modal analysis performed during the fatigue test:

- in general, there are no significant variations in the modal parameters throughout the fatigue test which can allow identification of damages;
- the only variation that could be significant is the splitting of the 20Hz mode in the last hammer test.

Then, regarding the structural dynamic analysis we can say that:

- the FE model of the blade is validated with the experimental results
- and since the 2nd optimization improved the MAC, it should be redone with a larger number of evaluations to see if there is a further improvement.

Future works could be:

1. Perform OMA during fatigue testing by using strain gauges since they are already used during the static test of the blade;
2. Further parameter optimizations with an higher number of evaluations;
3. Change the design variables of the optimization and include, for example, the composite layup.

Bibliography

- [1] Siemens Community. "omg! what is oma? operational modal analysis", 2020. <https://community.sw.siemens.com/s/article/OMG-What-is-OMA-Operating-Modal-Analysis>.
- [2] International Electrotechnical Commission. International standard iec 61400 wind turbine generator systems - part 23: full scale structural testing of rotor blades. *Wind Turbines-Part 1: Design Requirements*, 2014.
- [3] E. Di Lorenzo, S. Manzato, B. Peeters, V. Ruffini, P. Berring, P. U. Haselbach, K. Branner, and M. M. Luczak. Modal analysis of wind turbine blades with different test setup configurations. 2019.
- [4] Marcin Luczak, B. Peeters, S. Manzato, E. di Lorenzo, P. Z. Csurcsia, Kasper Reck-Nielsen, Peter Berring, Philipp Ulrich Haselbach, Kim Branner, and Valentina Ruffini. Integrated dynamic testing and analysis approach for model validation of an innovative wind turbine blade design. *Proceedings of ISMA2018 including USD2018 [248] Curran Associates*, 2018.
- [5] Bart Cauberghe. Applied frequency-domain system identification in the field of experimental and operational modal analysis, 2004.
- [6] D.J.Ewins. *Modal Testing: Theory, Practice and Application*. Research Studies Press LTD., 2000.
- [7] Bart Peeters, Herman Van der Auweraer, Patrick Guillaume, and Jan Leuridan. The polymax frequency-domain method: a new standard for modal parameter estimation? 2004.
- [8] Tomáš Harčík Miroslav Pastor, Michal Binda. Modal assurance criterion. *Elsevier*, 2012.

Bibliography

- [9] E.P. Tomasini. Lecture notes of "misure e controlli termotecnici". 2018/2019.
- [10] Siemens Community. "oma in simcenter testlab", 2020. <https://community.sw.siemens.com/s/article/OMA-in-Simcenter-Testlab>.